THE ASTROPHYSICAL JOURNAL, 544:522–539, 2000 November 20

RADIATIVE TRANSFER EFFECTS AND THE DYNAMICS OF SMALL-SCALE MAGNETIC STRUCTURES ON THE SUN

S. P. RAJAGURU[1,2] AND S. S. HASAN[1]
rajguru@physics.iisc.ernet.in
Received 2000 February 17; accepted 2000 June 20

ABSTRACT

The dynamical consequences of radiative energy transport on the evolution of gas confined to small-scale magnetic structures on the Sun are studied. Convective collapse, which transforms weak-field structures into intense structures of field strengths in the 1–2 kG range on the photosphere, is strongly influenced by radiative heating from the surroundings and cooling due to losses in the vertical direction. We first present analytic results in the quasi-adiabatic approximation to attempt a qualitative understanding of the influence of radiative effects on the convective stability of flux tubes. We demonstrate the destabilizing action of vertical radiative losses, that tend to enhance convective collapse and produce strong tubes at a relatively smaller horizontal scale than those expected from calculations based solely on horizontal radiative energy transport. Our calculations clearly point to an asymmetry between upflow and downflow perturbations—only the latter are amplified in the presence of vertical radiative transport. Using a realistic model of the solar atmospheric structure and treating radiative transfer in the diffusion and Eddington approximations, we next perform numerical stability analyses and produce size (flux)-strength relations for solar flux tubes. Our results provide a physical explanation for the observed flux-dependent (equivalently size-dependent) field strengths of the solar small-scale magnetic structures in the form of weak intranetwork and strong network components.

Subject headings: instabilities — MHD — radiative transfer — Sun: magnetic fields — Sun: photosphere

1. INTRODUCTION

Energy transport and momentum balance of gas motions in the subphotospheric and photospheric layers of the Sun are dominated by radiative energy losses. For instance, it is well known that these effects strongly influence the properties of granules (Spruit, Nordlund, & Title 1990). They can also be seen in numerical simulations of the solar convection (Cattaneo et al. 1991; Rast et al. 1993; Rast & Toomre 1993; Stein & Nordlund 1998). It is also well known that the horizontal radiative energy transport determines granular scales and their intensity contrasts (Musman & Nelson 1976; Nelson & Musman 1977, 1978). Such multidimensional effects of radiation are even more pronounced in the presence of magnetic fields (Spruit 1977; Knölker, Schüssler, & Weisshaar 1988), owing to modifications introduced to the thermal properties of the gas. These modifications stem from the inhibiting action of the magnetic field on the convective motions of the ionized gas (Biermann 1941). The initiation of convective collapse in a magnetic flux tube with an equipartition field strength (with respect to granular motions) is due to the insulation of the tube from the surrounding convective motions (Parker 1978): the gas confined to such structures is cooled faster than the surrounding gas owing to the unbalanced radiative losses through the surface cross section of the magnetic structure. Assuming that the horizontal optical thickness of the downflowing gas is sufficiently high so that radiative heating from the surroundings can be neglected, Parker (1978) reasoned that the downflow along the magnetic field lines proceeds almost adiabatically. The net effect of this nearly adiabatic downflow in the superadiabatically stratified gas below the photospheric surface is the evacuation of the upper layers of the flux tube, leading to an increase in the magnetic field strength to maintain pressure balance with the surroundings. However, it has been realized that the solar magnetic elements are small enough to be influenced strongly by the lateral influx of radiation (Spruit 1977), and many of the observed properties are determined by such effects: the excess continuum brightness, the structure, the size-dependent intensity contrasts, and the critical sizes for the transition from bright points to dark pores for magnetic structures are all determined by the action of radiative effects (Spruit & Zwaan 1981; Knölker et al. 1988; Knölker & Schüssler 1988). As regards the convective collapse process, for initial weak-field structures of small enough sizes, radiative heating from the surroundings (Hasan 1986; Venkatakrishnan 1986) renders the downflows significantly nonadiabatic, thereby reducing the efficiency of the collapse process. The main aim of our study is to examine quantitatively such size-dependent radiative effects and the associated observational consequences.

The small-scale concentrated flux elements are well known to have photospheric field strengths and sizes in the range 1–2 kG and 100–300 km (Howard & Stenflo 1972; Stenflo 1973; see the review by Stenflo 1994), respectively. These strong-field flux elements are found preferentially at the supergranular downflow regions and form the so-called *network*, which, at the chromospheric layers, causes excess emission in the Ca II K spectral lines, and this feature has long been identified as a proxy for magnetic activity. These network elements also play a dominant role in the dynamics of the overlying coronal gas. Observations have established that the flux elements comprising the network share uniform properties, such as their strength and other observational signatures, be it in the active region plages or in the quiet regions of the sun (Schüssler 1990, 1992). Most importantly, it has been found that the field strengths of these

[1] Indian Institute of Astrophysics, Koramangala, Bangalore-560 034, India.
[2] Joint Astronomy Program, Department of Physics, Indian Institute of Science, Bangalore-560 012, India.

strong-field structures show a very weak dependence on the flux per element, Φ: the active region network elements have Φ much higher than the quiet region ones, yet the field strengths are almost the same. This observational fact suggests that the formation and equilibrium process of these structures is unique and global. On the other hand, there are the inner network mixed-polarity weak-field structures whose field strengths have been measured recently (Keller et al. 1994; Lin 1995; Solanki et al. 1996) to have a typical value of 500 G, with the property that they have Φ typically less than 1×10^{17} Mx and with strengths strongly dependent on the flux. If the convective collapse of a weak-field tube is the global process responsible for the formation of the strong-field tubes (Parker 1978; Webb & Roberts 1978; Spruit & Zweibel 1979; Spruit 1979; Hasan 1983, 1984) that comprise the network with strengths weakly dependent on Φ, then we need to understand why tubes with smaller fluxes, viz., the inner network elements, do not collapse to kG strength. Efficient radiative exchange with the surroundings by a small flux tube (Hasan 1986; Venkatakrishnan 1986) offers a natural explanation. In particular, Venkatakrishnan (1986), using a simplified treatment of radiative effects, derived a size-strength relation for flux tubes on the Sun. Such a relation has been shown, recently, to agree qualitatively with observations (Solanki et al. 1996). In reality, the convective collapse process is not as simple as often modeled and occurs in a complicated environment dominated by flows and multidimensional radiative transfer. Radiative cooling associated with vertical radiative losses, which has not been so far modeled for a magnetic flux tube, plays an important role in enhancing convective downflows; this effect, thus, helps in producing strong tubes at a relatively smaller horizontal scale, consequently at magnetic flux values that are less than those expected from calculations based solely on horizontal radiative energy transport. We study the above-stated effects in detail enabling a quantitative comparison between the theoretical and observationally established properties of solar flux tubes.

We treat radiative transfer first in the diffusion approximation and subsequently in the more refined generalized Eddington approximation (Unno & Spiegel 1966). We compare the results for the two cases and delineate their validity. We note that a stability analysis that considers adiabatic displacements and their growth properties cannot distinguish between upward and downward perturbations, and, consequently, for the case of a flux tube in pressure equilibrium, it does not distinguish between field dispersal (upward displacements) and intensification (downward displacements) in the tube. In the present study, through the inclusion of nonadiabaticity due to both horizontal exchange and vertical radiative losses and by examining their competing influences, we show that a tube preferentially undergoes a collapse (Rajaguru 1999). Thus, we provide theoretical confirmation of the hypothesis (Parker 1978) that radiative losses would initiate a downward displacement that becomes unstable and leads to a collapse. We also check if the overstable oscillations driven by horizontal radiative exchange (Roberts 1976; Spruit 1979; Hasan 1985, 1986; Venkatakrishnan 1985; Massaglia, Bodo, & Rossi 1989) persist when vertical radiative losses are self-consistently taken into account.

The paper is organized as follows: in § 2 we present mathematical details and derive the necessary set of equations. In § 3 a quasi-adiabatic analysis of the equations is carried out. Using a local stability analysis, we derive results that bring out the basic physical features due to radiative transport and discuss the limiting behavior of the results. In § 4, we present numerical solutions to the full set of nonadiabatic equations derived in § 2; we discuss the implications of these results and present flux (size)-strength relations for small-scale solar tubes, which offers a meaningful comparison with observations. Finally, in § 5 the main conclusions of the study are summarized.

2. MATHEMATICAL FORMULATION

2.1. *Equations*

Let us consider a magnetic flux tube with an equipartition field strength, i.e., with a strength $B_{\rm eq} \equiv v_g(4\pi\rho)^{1/2} \approx 400$ G, which is obtained for a representative value of the photospheric granular flow speed of $v_g = 2$ km s^{-1} and a density $\rho = 3 \times 10^{-7}$ g cm^{-3}. We further assume that such tubes are thin enough to be adequately described by the quasi–one-dimensional *thin flux tube equations* that form a reduced set of MHD equations (Roberts & Webb 1978; Spruit 1981; Ferriz-Mas & Schüssler 1989). The equations are

$$\frac{\partial}{\partial t}\left(\frac{\rho}{B}\right) + \frac{\partial}{\partial z}\left(\frac{\rho v}{B}\right) = 0 , \tag{1}$$

$$\rho\left(\frac{\partial v}{\partial t} + v\,\frac{\partial v}{\partial z}\right) = -\,\frac{\partial p}{\partial z} + \rho g , \tag{2}$$

$$p + \frac{B^2}{8\pi} = p_e , \tag{3}$$

$$\frac{\partial p}{\partial t} + v\,\frac{\partial p}{\partial z} - \frac{\Gamma_1 p}{\rho}\left(\frac{\partial \rho}{\partial t} + v\,\frac{\partial \rho}{\partial z}\right) = -\,\frac{\chi_T}{\rho c_v T}\,\nabla\cdot\boldsymbol{F} , \tag{4}$$

$$Ba^2 = \text{const} , \tag{5}$$

where z denotes the vertical coordinate (positive downward), t denotes time, ρ is the mass density, v and B are the vertical components of the velocity and magnetic field strength on the tube axis, p is the gas pressure, T is the gas temperature, a is depth-dependent tube radius, $\boldsymbol{F}$ is the energy flux, g is the acceleration due to gravity (assumed constant and given by its value at the surface), and c_v is the specific heat at constant volume. Quantities with a subscript e, here and throughout the paper, refer to the external atmosphere. The quantities χ_T and Γ_1 are defined by

$$\chi_T = \left(\frac{\partial \ln p}{\partial \ln T}\right)_\rho , \tag{6}$$

$$\Gamma_1 = \chi_\rho \gamma = \chi_\rho\,\frac{c_p}{c_v} , \tag{7}$$

and

$$\chi_\rho = \left(\frac{\partial \ln p}{\partial \ln \rho}\right)_T . \tag{8}$$

The horizontal pressure balance condition given by equation (3) implies that the timescale for pressure adjustment over the cross section of the tube in response to the external pressure changes is small compared with all other relevant timescales in the problem. Pressure adjustment takes place approximately on a timescale for a magnetoacoustic wave

to cross the tube, which is typically a few seconds for a solar magnetic element.

The effects of radiation are incorporated in the energy equation (4). The total energy flux $\boldsymbol{F}$, in general, has contributions from all processes that contribute to energy transport in the flux tube. However, we treat only perturbations in the radiative flux $\boldsymbol{F}_R$ and neglect contributions from other flux perturbations. In the present thin tube approximation the divergence of the energy flux is

$$\nabla \cdot \boldsymbol{F} = 2F_{r1} + \frac{dF_z}{dz} , \tag{9}$$

where F_{r1} is the first-order term in the expansion of the radial component of the energy flux and r is the radial coordinate.[3]

2.1.1. *Radiative Transfer in the Diffusion Approximation*

The radiative flux $\boldsymbol{F}_R$ in the diffusion approximation is written as (see, e.g., Rybicki & Lightman 1979)

$$\boldsymbol{F}_R = -\frac{4\pi}{3\kappa\rho}\nabla\mathscr{B} = -\frac{16\sigma T^3}{3\kappa\rho}\nabla T , \tag{10}$$

where κ is the Rosseland mean absorption coefficient, $\mathscr{B} = \sigma T^4/\pi$ is the Planck function, and σ is the Stefan-Boltzmann constant. In this approximation, radiative energy transport essentially resembles heat conduction, with an "effective heat conductivity" K given by

$$K = 16\sigma T^3/3\kappa\rho . \tag{11}$$

Expanding $\mathscr{B}$ about the axis of the tube we find the components of radiative flux to be

$$F_{R,r1} = -\frac{8\pi\mathscr{B}_2}{3\kappa\rho} , \quad F_{R,z} = -\frac{4\pi}{3\kappa\rho}\frac{d\mathscr{B}}{dz} ,$$

where $\mathscr{B}_2$ is the second-order term in the expansion of $\mathscr{B}$ and can be estimated by demanding

$$\mathscr{B}(a, z) = \mathscr{B}_e(z) ,$$

which yields

$$\mathscr{B}_2 = \frac{\mathscr{B}_e\mathscr{B}}{a^2} = \frac{\sigma(T_e^4 - T^4)}{\pi a^2} . \tag{12}$$

Equation (9) can then be written for radiative flux in the diffusion approximation as

$$\nabla \cdot \boldsymbol{F}_R = -\frac{16\sigma(T_e^4 - T^4)}{3\kappa\rho a^2} - \frac{d}{dz}\left(\frac{16\sigma T^3}{3\kappa\rho}\frac{dT}{dz}\right) . \tag{13}$$

2.1.2. *Radiative Transfer in the Eddington Approximation*

We utilize the three-dimensional generalization of the Eddington approximation (Unno & Spiegel 1966) to derive a transfer equation appropriate for a thin magnetic flux tube, following Hasan (1988). The radiative flux $\boldsymbol{F}_R$ in this approximation is written as

$$\boldsymbol{F}_R = -\frac{4\pi}{3\kappa\rho}\nabla J . \tag{14}$$

[3] Regularity at $r = 0$ and symmetry of the problem demands that radial components of vectors retain only the odd terms and the scalars and axial components of vectors the even terms, in the expansion about the axis (Ferriz-Mas & Schüssler 1989).

An equation for the mean intensity J is obtained by using the above expression for $\boldsymbol{F}_R$ in the following relation (Unno & Spiegel 1966):

$$\nabla \cdot \boldsymbol{F}_R = 4\pi\kappa\rho(S - J) , \tag{15}$$

where S is the source function, which we equate to the Planck function $\mathscr{B}$ (i.e., we assume local thermodynamic equilibrium [LTE]). Hence, $S = \sigma T^4/\pi$. The above equation is essentially the transfer equation integrated over solid angle and frequency for a gray medium. In the present case of a slender tube the zeroth-order reduction of the above two equations yields (Hasan 1988)

$$\frac{1}{3}\frac{\partial^2 J}{\partial\tau^2} + \frac{4}{3}\left(\frac{J_e - J}{\tau_a^2}\right) = J - S , \tag{16}$$

where $d\tau = \kappa\rho\, dz$, $\tau_a = \kappa\rho a$, and J_e is the mean intensity in the external medium that satisfies

$$\frac{1}{3}\frac{\partial^2 J_e}{\partial\tau_e^2} = J_e - S_e , \tag{17}$$

where $d\tau_e = \kappa_e\rho_e dz$ is the optical depth element in the external medium. The calculation of the radiation field fluctuations and their coupling to the hydrodynamic perturbations are done conveniently using the following first-order moment forms of the above equations. The transfer equation (16) can be written as

$$\frac{dJ}{d\tau} = -3\mathscr{H} , \tag{18}$$

$$\frac{d\mathscr{H}}{d\tau} - \frac{4}{3}\left(\frac{J_e - J}{\tau_a^2}\right) = S - J , \tag{19}$$

while, for the external medium, equation (17) can be written as

$$\frac{dJ_e}{d\tau_e} = -3\mathscr{H}_e , \tag{20}$$

$$\frac{d\mathscr{H}_e}{d\tau_e} = S_e - J_e . \tag{21}$$

Here $\mathscr{H}$ is the Eddington flux, related to the flux $F_{R,z}$ by

$$F_{R,z} = 4\pi\mathscr{H} . \tag{22}$$

2.2. *Equilibrium*

We consider an initial equilibrium state of a slender magnetic flux tube embedded in a plane-parallel stratified atmosphere that is in hydrostatic and energy equilibrium. We assume that the temperatures in the flux tube and the external atmosphere are the same at each height. The equation for hydrostatic equilibrium that is satisfied by both the flux tube and the external atmospheres is

$$\frac{dp}{dz} = \rho g . \tag{23}$$

The energy equilibrium conditions for the flux tube and the external atmosphere are, respectively,

$$\nabla \cdot \boldsymbol{F} = 2F_{r1} + \frac{dF_z}{dz} = 0 \tag{24}$$

and

$$\nabla \cdot \boldsymbol{F}_e = \frac{dF_{z,e}}{dz} = 0 \,. \tag{25}$$

Furthermore, we assume pressure balance given by equation (3). The equilibrium stratification of the external medium that is used here is the one determined to match the VAL-*C* (Vernazza, Avrett, & Loeser 1981) model for the photosphere and the higher layers with the convection zone constructed as explained in Hasan & Kalkofen (1994) and Hasan, Kneer, & Kalkofen (1998). The convection zone structure in this model differs slightly from that of Spruit (1977), owing to refinements in the treatments of radiative transfer and mixing-length formalism. This model satisfies the hydrostatic and energy equilibrium conditions given by equations (23) and (25). Saha's equation is used to determine μ, the mean molecular weight, and the various thermodynamic quantities such as c_v are determined following Mihalas (1967). The Rosseland mean opacities are calculated by interpolation from the tables of R. L. Kurucz (1993, private communication; see Hasan & Kalkofen 1994) for the upper layers of the atmosphere and from those of Rogers & Iglesias (1992) for the deeper regions. The depth dependence of adiabatic temperature gradient $\nabla_a = (\partial \ln T/\partial \ln p)_{\rm ad}$ and the actual temperature gradient $\nabla = \partial \ln T/\partial \ln p$ are shown in the upper panel of Figure 1 and that of superadiabaticity $\delta = \nabla - \nabla_a$ is shown in the lower panel of Figure 1.

The radius of the flux tube is found from the flux conservation condition given by equation (5). The condition of temperature equilibrium implies that $\beta = 8\pi p/B^2$ is constant with depth. Hence, it follows that the pressure and density inside the tube are related to those in the external atmosphere by

$$p = \frac{\beta}{1+\beta}\, p_e \,, \tag{26}$$

$$\rho = \frac{\beta}{1+\beta}\, \rho_e \,. \tag{27}$$

In the diffusion approximation, because of the assumption of temperature equilibrium, there is no net radiative flux across the tube from the external atmosphere; i.e., $F_{R,r1} = 0$. In the Eddington approximation, the mean radiation intensity J_e as a function of depth for the solar model used is determined by solving equation (17). This we do numerically, using finite differences with the following upper and lower boundary conditions:

$$\frac{1}{\sqrt{3}}\frac{\partial J_e}{\partial \tau_e} = J_e \tag{28}$$

and

$$\frac{1}{\sqrt{3}}\frac{\partial J_e}{\partial \tau_e} = -J_e + I_e^+ \,, \tag{29}$$

respectively, where I_e^+ is the radiation intensity in the upward direction, which, in the diffusion approximation, is

$$I_e^+ = S_e + \frac{1}{\sqrt{3}}\frac{1}{\kappa_e \rho_e}\frac{\partial S_e}{\partial z} \,. \tag{30}$$

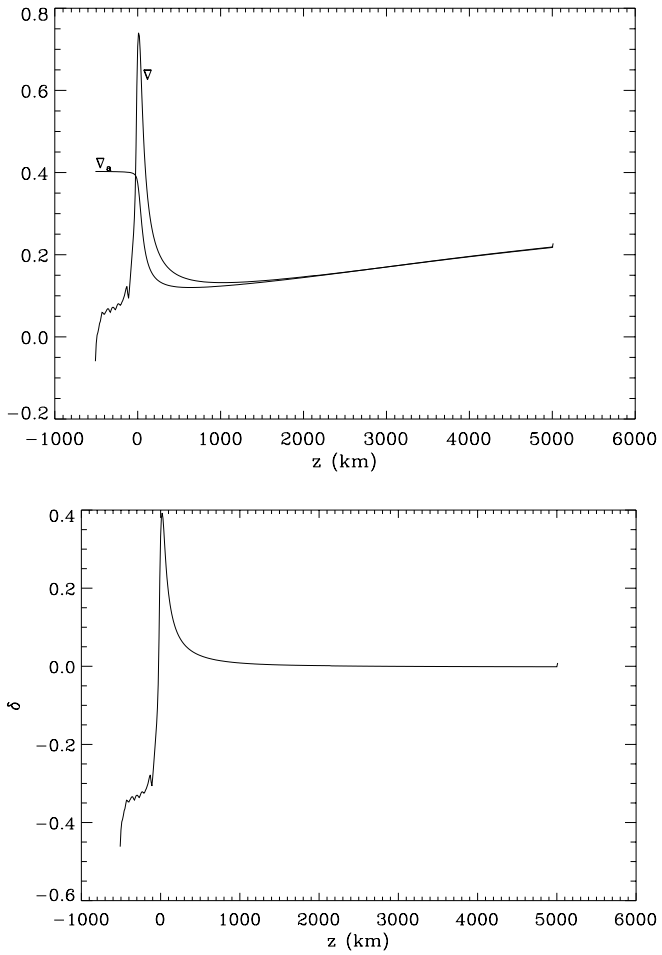

FIG. 1.—Depth dependence of (*top*) the adiabatic and actual temperature gradients ∇_a and ∇, respectively, and (*bottom*) the superadiabaticity $\delta = \nabla - \nabla_a$.

The mean intensity J inside the tube is now determined by inserting the values of J_e determined above in equation (16) and solving it with the same set of boundary conditions as that for the external medium. We place the upper boundary in the chromosphere at the temperature minimum ($z_{\rm top} = -500$ km) and the lower boundary at a depth of 5000 km in the convection zone with the photospheric surface ($\tau_e = 1$) chosen as $z = 0$. The depth variation of $\nabla \cdot \boldsymbol{F}_R$ is shown in Figure 2 (where $\boldsymbol{F}_R$ is calculated in the Eddington and diffusion approximations, respectively), which reveals that this quantity is overestimated in the optically thin layers by the diffusion approximation. The radiative flux inside the tube, calculated here, is an approximate representation of the real situation for which one needs to construct the atmospheric structure inside the tube consistently by solving the (magneto)hydrostatic equation along with the radiative transfer equation. Since our main concern here is not the detailed equilibrium structure, we have approximated the temperature structure inside to be identical with that in the external medium. This is not very different from the real situation as can be seen from elaborate analyses involving more refined treatments of radiative transfer (Steiner 1990; Hasan & Kalkofen 1994; Hasan, Kalkofen, & Steiner 1999), which reveal that the temperature difference at equal geometrical levels is generally small except in the thin surface layers. The effect of such a temperature difference is likely to

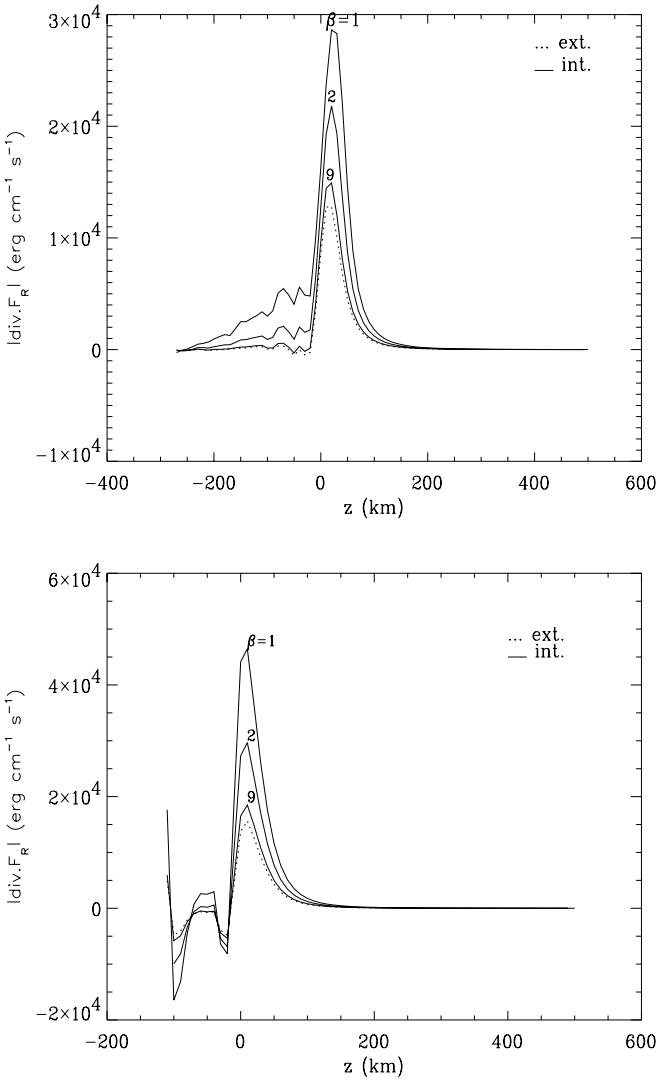

FIG. 2.—Magnitude of $\nabla \cdot \boldsymbol{F}_R$, (*top*) in the Eddington approximation and (*bottom*) in the diffusion approximation, which is a measure of radiative losses as a function of depth for different values of β.

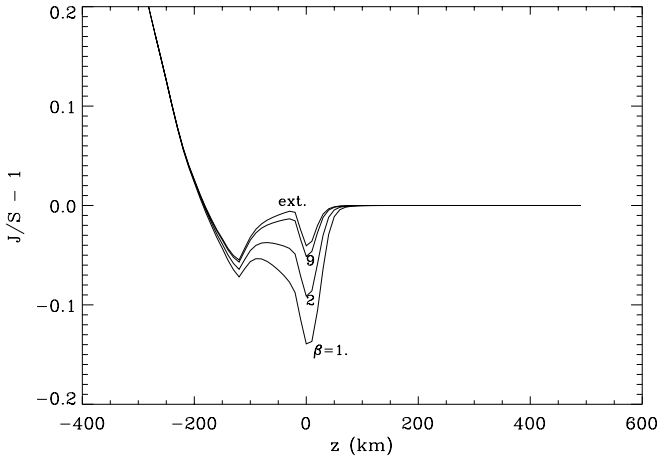

FIG. 3.—Depth dependence of $\Delta_c = J/S - 1$, which measures the departure of the mean intensity from the Planck function, for three representative values of β that are marked in the panels.

have a negligible influence on the growth rates and frequencies of the modes of the flux tube. The main difference between the present case of Eddington approximation and the diffusion approximation is represented by the quantity Δ_c, defined as $\Delta_c = J/S - 1$, which measures the departure of the mean intensity from the source function (the Planck function by assumption). This quantity is always small and has finite values only in the upper photospheric layers close to optical depth unity and is zero in the deep layers that are optically thick. Yet, as we show later in this paper, this quantity shows an appreciable stabilizing influence on the unstable modes of the tube. Figure 3 shows the variation of Δ_c with z. We find that the stronger the tube (or equivalently, the smaller the values of β), the larger is the departure from the Planck function for the mean intensity inside the tube.

2.3. *Linear Stability: Perturbed Equations*

Small amplitude fluctuations are imposed on the equilibrium configuration, described above. We linearize the thin tube equations (1)–(4) and (9) with an assumption that the external atmosphere is unaffected by the motions inside the tube. Specifically, we neglect the Eulerian perturbations in the external pressure and in the nonradiative energy fluxes, such as the convective energy flux. With these assumptions, small amplitude perturbations inside the tube obey the following equations:

$$\frac{\partial \xi}{\partial z} = \frac{B'}{B} - \frac{\rho'}{\rho} - \left[\frac{d(\ln \rho)}{dz} - \frac{d(\ln B)}{dz}\right]\xi , \tag{31}$$

$$\frac{\partial^2 \xi}{\partial t^2} = -Hg \frac{\partial}{\partial z}\left(\frac{p'}{p}\right) - g\left(\frac{p'}{p} - \frac{\rho'}{\rho}\right), \tag{32}$$

$$\frac{B'}{B} = -\frac{\beta}{2}\frac{p'}{p}, \tag{33}$$

$$\frac{\partial}{\partial t}\left(\frac{p'}{p}\right) - \Gamma_1 \frac{\partial}{\partial t}\left(\frac{\rho'}{\rho}\right) + \frac{N^2 \Gamma_1}{g}\frac{\partial \xi}{\partial t} = -\frac{\chi_T}{\rho c_v T}\nabla \cdot \boldsymbol{F}'_R , \tag{34}$$

where ξ denotes the vertical displacement, H is the pressure scale height, and N^2 is the squared Brunt-Väisälä frequency,

$$N^2 = g\left(\frac{1}{\Gamma_1}\frac{d\ln p}{dz} - \frac{d\ln \rho}{dz}\right). \tag{35}$$

The divergence of the radiative flux perturbations, in the diffusion and Eddington approximations, is calculated using the basic equations given in §§ 2.1.1 and 2.1.2, respectively. The resulting equations are summarized below in the following subsections; we refer the reader to Rajaguru (1999), for details.

2.3.1. *Diffusion Approximation*

In this case, using equation (13), we find

$$\nabla \cdot \boldsymbol{F}'_R = \frac{4KT}{a^2}\frac{T'}{T} + F_z \frac{\partial}{\partial z}\left(\frac{F'_z}{F_z}\right) + \frac{dF_z}{dz}\frac{F'_z}{F_z}, \tag{36}$$

where the first term on the right-hand side corresponds to lateral heat exchange due to thermal fluctuations and the second and third terms describe the effects of perturbations in the vertical radiative energy flux (F_z and F'_z hereafter denote the vertical radiative flux and its perturbation,

respectively). From equation (10) we find

$$\frac{F_z'}{F_z} = \left(\frac{d\ln T}{dz}\right)^{-1} \frac{\partial}{\partial z}\left(\frac{T'}{T}\right) + 4\,\frac{T'}{T} - \left(\frac{\kappa'}{\kappa} + \frac{\rho'}{\rho}\right), \quad (37)$$

Fourier decomposition in time of all the fluctuating variables, i.e., with the time dependence in the separable form $f'(z)\exp(-i\omega t)$, for a typical perturbation variable $f'(z, t)$, yields the following set of equations in nondimensional form (Rajaguru 1999):

$$\frac{d\xi}{dZ} = \frac{1}{H}\left(\frac{dH}{dZ} - \frac{1}{2}\right)\xi - \left(\frac{\beta}{2} + \frac{1}{\chi_\rho}\right)\frac{p'}{p} + \frac{\chi_T}{\chi_\rho}\frac{T'}{T}, \quad (38)$$

$$\frac{d}{dZ}\left(\frac{p'}{p}\right) = \frac{\Omega^2}{H}\,\xi - \frac{(\chi_\rho - 1)}{\chi_\rho H}\frac{p'}{p} - \frac{\chi_T}{\chi_\rho H}\frac{T'}{T}, \quad (39)$$

$$\frac{d}{dZ}\left(\frac{T'}{T}\right) = \frac{d\ln T}{dZ}\left(\kappa_p + \frac{1}{\chi_\rho}\right)\frac{p'}{p} - \frac{d\ln T}{dZ}\left(4 - \kappa_T + \frac{\chi_T}{\chi_\rho}\right)\frac{T'}{T} + \frac{d\ln T}{dZ}\frac{F_z'}{F_z}, \quad (40)$$

$$C\,\frac{d}{dZ}\left(\frac{F_z'}{F_z}\right) = -i\Omega\,\frac{\mathcal{N}^2\Gamma_1}{\chi_T}\,\xi + i\Omega\,\frac{(\gamma - 1)}{\chi_T}\,\frac{p'}{p} + (4\epsilon - i\Omega\gamma)\,\frac{T'}{T} - C\,\frac{d\ln F_z}{dZ}\,\frac{F_z'}{F_z}, \quad (41)$$

where

$$Z = \frac{z}{L}, \quad (42)$$

$$\Omega = \omega\tau_d, \quad (43)$$

$$\tau_d = \left(\frac{L}{g}\right)^{1/2}, \quad (44)$$

and

$$\mathcal{N}^2 = N^2\tau_d^2 \quad (45)$$

is the nondimensional squared Brunt-Väisälä frequency. Here, the length scale L is taken to be the depth extension of the tube from $z = 0$. The quantities κ_p and κ_T are defined by

$$\kappa_p = \left(\frac{\partial\ln\kappa}{\partial\ln p}\right)_T, \quad \kappa_T = \left(\frac{\partial\ln\kappa}{\partial\ln T}\right)_p. \quad (46)$$

All the quantities appearing in the above equations are dimensionless; the displacement ξ and the scale height H are in units of L. The nonadiabaticity parameter C is the ratio of the free-fall time τ_d to the thermal timescale $\tau_{\rm th}$ (Jones 1970; Antia & Chitre 1979):

$$C = \frac{\tau_d}{\tau_{\rm th}}, \quad (47)$$

with

$$\tau_{\rm th} = \frac{\rho c_v T L}{F}, \quad (48)$$

where F is the magnitude of the vertical component of the radiative flux. The timescale $\tau_{\rm th}$ represents the thermal timescale in which radiative relaxation takes place over the length of the tube. In addition, ϵ is given by

$$\epsilon = \frac{\tau_d}{\tau_r}, \quad (49)$$

where

$$\tau_r = \frac{\rho c_v a^2}{K} \quad (50)$$

is the lateral radiative exchange timescale. We note that the timescales $\tau_{\rm th}$ and τ_r are depth dependent and so are the parameters C and ϵ.

2.3.2. *Eddington Approximation*

In this approximation, the divergence of $\boldsymbol{F}_R$ is found using the perturbed form of equation (15), which yields

$$\boldsymbol{\nabla}\cdot\boldsymbol{F}_R = \frac{dF_R'}{dz} = 4\pi\kappa_a\rho(S' - J') + \boldsymbol{\nabla}\cdot\boldsymbol{F}_R\left(\frac{\kappa'}{\kappa} + \frac{\rho'}{\rho}\right). \quad (51)$$

Expanding ρ'/ρ and κ'/κ in terms of T'/T and p'/p and using $S' = T'dS/dT = 4ST'/T$, we have

$$\boldsymbol{\nabla}\cdot\boldsymbol{F}_R' = k_1\,\boldsymbol{\nabla}\cdot\boldsymbol{F}_R\,\frac{p'}{p} + (k_2\,\boldsymbol{\nabla}\cdot\boldsymbol{F}_R + 16\pi\kappa\rho S)\,\frac{T'}{T} - 4\pi\kappa\rho J', \quad (52)$$

where

$$k_1 = \frac{1}{\chi_\rho} + \kappa_p, \quad (53)$$

$$k_2 = \kappa_T - \frac{\chi_T}{\chi_\rho}, \quad (54)$$

which when substituted into equation (34) yields the desired equation relating the mean intensity perturbations to the thermodynamic perturbations:

$$a_1\,\frac{p'}{p} + a_2\,\frac{T'}{T} + i\Omega\Gamma_1\,\mathcal{N}^2\xi + q\chi_T(1 + \Delta_c)\,\frac{J'}{J} = 0, \quad (55)$$

where

$$a_1 = i\Omega(1 - \gamma) + q\Delta_c\,\chi_T\,k_1, \quad (56)$$

$$a_2 = i\Omega\gamma\chi_T - q\chi_T(4 - \Delta_c\,k_2), \quad (57)$$

and

$$q = \frac{\tau_d}{\tau_N}, \quad (58)$$

$$\tau_N = \frac{c_v T}{4\pi\kappa S}, \quad (59)$$

is the radiative relaxation time in the optically thin limit (i.e., with Newton's law of cooling; Unno & Spiegel 1966). Equation (55) is used to replace temperature perturbations T'/T in the remaining equations. The perturbation in the mean intensity J' is determined by perturbing and linearizing the transfer equation (16). Here we use the equivalent equations (18) and (19) to relate the radiation field perturbations J'/J and $\mathcal{H}'/\mathcal{H}$ to the hydrodynamic perturbations ξ, p'/p. After lengthy but straightforward algebra, we arrive

at the following final set of equations:

$$\frac{d\xi}{dZ} = \left[\frac{1}{H}\left(\frac{dH}{dZ} - \frac{1}{2}\right) - i\,\frac{\Omega\mathcal{N}^2\Gamma_1\chi_T}{\chi_\rho a_2}\right]\xi - \left(\frac{1}{\chi_\rho} + \frac{\beta}{2} - \frac{\chi_T a_1}{\chi_\rho a_2}\right)\frac{p'}{p} - q\,\frac{(1+\Delta_c)\chi_T^2}{a_2\chi_\rho}\,\frac{J'}{J}\,, \quad (60)$$

$$\frac{d}{dZ}\left(\frac{p'}{p}\right) = \frac{1}{H}\left(\Omega^2 + i\,\frac{\Omega\mathcal{N}^2\Gamma_1\chi_T}{\chi_\rho a_2}\right)\xi + \frac{1}{H}\left[\frac{(1-\chi_\rho)}{\chi_\rho} + \frac{\chi_T a_1}{\chi_\rho a_2}\right]\frac{p'}{p} + q\,\frac{(1+\Delta_c)\chi_T^2}{a_2\chi_\rho H}\,\frac{J'}{J}\,, \quad (61)$$

$$\frac{d}{dZ}\left(\frac{J'}{J}\right) = -i\,\frac{\Omega\mathcal{N}^2\Gamma_1 k_2}{a_2}\,\frac{d\ln J}{dZ}\,\xi + \left(k_1 - \frac{k_2 a_1}{a_2}\right)\times\frac{d\ln J}{dZ}\,\frac{p'}{p} - \left[1 + q\,\frac{(1+\Delta_c)\chi_T k_2}{a_2}\right]\times\frac{d\ln J}{dZ}\,\frac{J'}{J} + \frac{d\ln J}{dZ}\,\frac{H'}{H}\,, \quad (62)$$

$$C\,\frac{d}{dZ}\left(\frac{\mathscr{H}'}{\mathscr{H}}\right) = -i\,\frac{\Omega\mathcal{N}^2\Gamma_1}{a_2}\,(a_3 k_2 + q)\xi + \left(a_3 k_1 - \frac{a_1 a_3 k_2}{a_2} - q\,\frac{a_1}{a_2} + 8\epsilon\Delta_t\right)\frac{p'}{p} - \left[q\,\frac{(1+\Delta_c)\chi_T}{a_2}\,(q + a_3 k_2) + (1+\Delta_c)(\epsilon + q)\right]\times\frac{J'}{J} - C\,\frac{d\ln\mathscr{H}}{dZ}\,\frac{\mathscr{H}'}{\mathscr{H}}\,, \quad (63)$$

where

$$a_3 = C\,\frac{(S-J)\Lambda}{\mathscr{H}} + \epsilon\Delta_t \quad (64)$$

and

$$\Delta_t = \frac{J - J_e}{S} \quad (65)$$

is the ratio of the excess of the mean intensity inside the tube to the Planck function. It is straightforward to verify that the above set of equations yields the correct limiting forms in the optically thick and thin cases. The equations for an optically thick atmosphere correspond to taking the limit $\kappa\rho \to \infty$ and replacing the mean intensity by the Planck function. The optically thin case is obtained in the limit of mean intensity perturbations inside the tube $J'/J \to 0$.

The adiabatic limit occurs, in the systems of equations (38)–(41) and (60)–(63), separately, when ϵ and $C \to 0$ (i.e., as τ_r and $\tau_{\rm th} \to \infty$). The resulting second-order system has been treated in Webb & Roberts (1978), Spruit & Zweibel (1979), and Unno & Ando (1979).

The limit of $C \to 0$ (i.e., when $\tau_{\rm th} \to \infty$, but not τ_r) in the energy equation given by equation (41) yields

$$-\frac{N^2\Gamma_1}{g\chi_T}\,\xi + \frac{(\gamma-1)}{\chi_T}\,\frac{p'}{p} - \left(\gamma + i\,\frac{4\epsilon}{\Omega}\right)\frac{T'}{T} = 0\,. \quad (66)$$

This equation is applicable when nonadiabaticity is solely due to lateral exchange of radiation between the tube and its surroundings; note that τ_r is the thermal relaxation time in the optically thick limit, which follows from the following exact formula (first derived by Spiegel 1957) by replacing the inverse of the wavenumber k by a, the tube radius, and taking the limit of $\kappa\rho a \to \infty$ (Hasan 1986):

$$\tau_s = \frac{c_v}{16\kappa\sigma T^3}\,[1 - (\kappa\rho a)\,\cot^{-1}(\kappa\rho a)]^{-1}\,. \quad (67)$$

The optically thin limit ($\kappa\rho a \ll 1$) in the above formula gives the timescale τ_N given by equation (59). Now, the use of equation (66) to replace the temperature perturbations in equations (38) and (39) leads to a second-order system, which has been treated by Hasan (1986). This same second-order system is arrived at when the mean intensity perturbations $J'/J \to 0$ in the Eddington approximation equations (60)–(63). Solutions of this system for isothermal stratifications have been obtained by (Webb & Roberts 1980).

Before presenting numerical solutions, in § 4, to the sets of equations derived above using the diffusion and the Eddington approximations, we first simplify the equations under the quasi-adiabatic approximation in order to gain a clear physical understanding of the various effects under study.

3. QUASI-ADIABATIC APPROXIMATION FOR A THIN FLUX TUBE

3.1. *Equations*

The quasi-adiabatic approximation, which qualitatively captures the physical effects associated with both vertical and horizontal energy transport, has the advantage that the number of differential equations is reduced effectively to two. This approximation is effected by using the adiabatic relations among the variables, i.e., using those obtained in the limit of ϵ and $C \to 0$ applied to the set of equations (38)–(41), to evaluate the right-hand side of equation (37). This procedure yields the following evaluation (see the Appendix for details) of the energy equation written in terms of Lagrangian variables (prefixed with the symbol δ):

$$(\gamma\theta\tau_d + 4\epsilon)\,\frac{\delta s}{c_v} = \frac{\gamma D_3(z)}{H}\,\xi + \gamma D_4(z)\,\frac{\delta p}{p}\,, \quad (68)$$

where δs is the Lagrangian perturbation in entropy and we have used a time dependence of the form $e^{\theta t}$, for convenience. The coefficients $D_3(z)$ and $D_4(z)$ are dimensionless functions of θ and the various parameters determining the equilibrium atmospheric structure and are given in the Appendix. Use of this equation in the Lagrangian forms of equations (38) and (39) and straightforward simplification yield the following second-order equation for ξ:

$$\frac{d^2\xi}{dz^2} + \frac{P}{2H}\,\frac{d\xi}{dz} + \left(\frac{R}{H^2} + \frac{Q}{H}\right)\xi = 0\,, \quad (69)$$

where

$$P = 1 - 2\left(\frac{\chi_T D_3}{q\chi_\rho} + \frac{HM'}{M}\right), \quad (70)$$

$$R = I(\nabla - 1) + \frac{M}{2} + \frac{\beta}{2}\,(M - I)\,, \quad (71)$$

$$Q = \frac{IM'}{M} - I' - \frac{M\Omega^2}{L}\,, \tag{72}$$

$$I = \frac{1+\beta}{2} + \frac{\chi_T}{q\chi_\rho}\, D_3(z)\,, \tag{73}$$

$$M = \frac{\beta}{2} + \frac{1}{\Gamma_1} - \frac{\chi_T}{q\chi_\rho}\, D_4(z)\,, \tag{74}$$

and

$$q = \gamma\theta\tau_d + 4\epsilon\,. \tag{75}$$

Here the prime symbol denotes a derivative with respect to z (e.g., $M' \equiv dM/dz$). In the limit $C \to 0$, the above equation reduces to the case where the only nonadiabaticity is through the lateral exchange of radiation and is the same as treated by Hasan (1986). In the adiabatic limit, i.e., when both ϵ and $C \to 0$, it reduces to the form derived by Spruit & Zweibel (1979). The above second-order differential equation does not lend itself to an analytic solution, because of the complicated forms of the various coefficients appearing in it. To gain a clear physical understanding of the various effects of radiative energy exchange embodied in it, we carry out a "local analysis" that leads to a dispersion relation that enables us to delineate these effects.

3.2. *Solutions in the Local Approximation*

In the so-called local approximation, we assume that the coefficients of the displacement and their derivatives in equation (69) vary weakly with depth; this corresponds to assuming a locally homogeneous atmosphere. Thus, the various quantities appearing in the equations have values corresponding to a particular height in the atmosphere, and here for convenience we redefine the scaling length L to be the local scale height H. Therefore, the length scale appearing in the thermal timescale $\tau_{\rm th}$ is the local scale height and hence C is the ratio of the local free-fall time $\tau_d = (H/g)^{1/2}$ to the local thermal timescale. Furthermore, we neglect contributions from the perturbations in the opacity to the dynamic perturbations; i.e., there is no κ mechanism operating inside the flux-tube–confined gas. Under these approximations, the various coefficients in equation (69) become constants and the application of rigid boundary conditions $\xi = 0$ at $z = 0$ and at $z = D$, where D is the length of the tube, leads to the following dispersion relation for the dimensionless eigenvalue $\Theta = \theta\tau_d$:

$$S_4\,\Theta^4 + \Theta^3 + S_2\,\Theta^2 + S_1\,\Theta + S_0 = 0\,, \tag{76}$$

where

$$S_4 = C\sigma_4\,, \tag{77}$$

$$S_2 = \epsilon\eta_2 + C\sigma_2\,, \tag{78}$$

$$S_1 = \frac{\gamma}{\delta_c}\left[b_0 - \frac{(1+\beta)\delta}{2}\right], \tag{79}$$

$$S_o = \epsilon\eta_o + C\sigma_o\,, \tag{80}$$

and

$$\sigma_4 = -\frac{\nabla_a}{\gamma\nabla}\,, \tag{81}$$

$$\eta_2 = \frac{4}{\delta_c}\left(1 + \frac{\beta}{2}\right), \tag{82}$$

$$\sigma_2 = \frac{\delta}{\delta_c\nabla}\left[\frac{(1+\beta)}{2}\,\nabla_a + \frac{\nabla}{2} + \frac{1}{8}\right] + \frac{1}{\gamma}\,\frac{\nabla_a}{\nabla} + \frac{1+\beta}{2}\left[\nabla - \frac{(2\beta+3)}{4}\right]\frac{1}{\delta_c} - Q_r\left(\frac{2}{\gamma} - \frac{1}{4}\,\frac{\nabla_a}{\delta_c\nabla}\right), \tag{83}$$

$$\eta_o = \frac{4b_0 + \nabla(1-4\nabla)}{\delta_c}\,, \tag{84}$$

$$\sigma_o = -\frac{(1+\beta)}{4\delta_c}\left[\frac{1}{4} + \nabla + (1+\beta)\nabla_a\right]\frac{\delta}{\nabla} + Q_r\,\frac{1+\beta}{2\delta_c}\left[\delta\left(1 + \frac{1}{4\nabla}\right) + \nabla + \frac{1}{\gamma} - \frac{3}{4}\right], \tag{85}$$

$$\delta_c = 1 + \frac{\gamma\beta}{2}\,, \tag{86}$$

$$b_0 = \frac{1}{16} + \frac{n^2\pi^2H^2}{D^2}\,, \tag{87}$$

n being the harmonic order of the perturbations. In the above,

$$Q_r = H\,\frac{d\ln F_R}{dz}\,, \tag{88}$$

which is a measure of vertical radiative losses (equivalently, a measure of departure from radiative equilibrium) and is negative because $|F_R|$ decreases as z increases. The greater the radiative losses the larger the magnitude of Q_r. In the limit $C \to 0$, i.e., when the vertical radiative transfer is switched off, the above dispersion relation becomes a cubic equation that describes the effects of horizontal exchange alone; furthermore, it is seen that, in the limit of isothermal background stratification (i.e., when $\nabla = 0$), the dispersion relation reduces to the following form derived by Venkatakrishnan (1986):

$$\Theta^3 + s_2\,\Theta^2 + s_1\,\Theta + s_o = 0\,, \tag{89}$$

where

$$s_2 = \frac{4\epsilon}{\delta_c}\left(1 + \frac{\beta}{2}\right), \tag{90}$$

$$s_1 = \frac{\gamma}{\delta_c}\left[b_0 - \frac{(1+\beta)(1-\gamma)}{2\gamma}\right], \tag{91}$$

$$s_o = \frac{4\epsilon b_0}{\delta_c}\,. \tag{92}$$

It describes the linear evolution of a gas element constrained to move in the vertical direction, guided by a thin flux tube that exchanges radiative heat with its surroundings. We note here the similarity between the one-dimensional (vertical) motions of the flux-tube–confined gas element and a model overstable oscillator studied by Moore & Spiegel (1966): in the linear limit, this overstable oscillator obeys the same dispersion relation as the present one (eq. [89]); the restoring force in the oscillator of Moore & Spiegel is provided by a spring attached to the gas element, whereas here it is provided by the magnetic field, and the dissipative force is the same, viz., horizontal heat exchange under Newton's law of cooling. Thus, the generalization that we have achieved here through the fourth-order dispersion relation (76) can also be applied to Moore & Spiegel's

oscillator that cools in the vertical direction while being heated horizontally. Equation (89), which brings out in a simple way the size-dependent collapse of the tubes, was solved numerically by Venkatakrishnan (1986) to obtain a relationship between the size and strength for stable solar tubes. Here, we derive an approximate analytic relation between ϵ (i.e., the size of the tube) and critical values of β at which the convective instability sets in, through a straightforward analysis of the transition from oscillatory to convective behavior contained in the solutions to equation (89).

The limit $\epsilon = 0$ in equation (89) gives the adiabatic solution,

$$\Theta_{ad} = \pm(-s_1)^{1/2} , \tag{93}$$

which shows that, if s_1 is positive, i.e., if β is less than a critical value $\beta_c = 2b_o/\delta - 1$, then the tube is convectively stable and exhibits undamped oscillations with frequency Θ_{ad} (Webb & Roberts 1978). The inclusion of radiative exchange introduces two new effects. First, Θ_{ad} becomes complex, transforming the adiabatic oscillatory mode into a growing mode (overstable) and introducing damping to the convective mode. To first order in ϵ, this behavior is exhibited by the complex roots of equation (89),

$$(\Theta_i)_{1,2} = \Theta_{ad} + \frac{s_o - s_1 s_2}{2s_1} . \tag{94}$$

Second, there is introduced a new thermal mode corresponding to the real root,

$$(\Theta_i)_3 = -\frac{s_o}{s_1} . \tag{95}$$

Since s_o is always positive, this thermal mode is damped when s_1 is positive and growing when it is negative; this means that the thermal mode is destabilized when the stratification is convectively unstable, i.e., when the field strength is less than the adiabatic stability limit (or $\beta > \beta_c$). Furthermore, the growth rate of this thermal mode decreases as the horizontal size of the flux tube increases (i.e., as ϵ decreases). This property reveals that the mode derives its energy from the horizontal radiative exchange, and since it is of the convective type (monotonic growth), it can be regarded as a slow upward motion (in analogy with a similar solution of Moore & Spiegel's overstable oscillator). This thermal mode and its above-mentioned behavior have been noted earlier (Hasan 1986).

Considering the solutions given by equation (94), it is easily noted that, to first order in ϵ, the lateral radiative exchange introduces either damping or amplification without affecting the frequencies of the oscillatory mode and thus does not determine the transition from oscillatory to convective behavior, which is still set by the adiabatic limit. This shows that the size-dependent onset of the convective instability of a tube is an effect at least of order 2 in ϵ. Such a dependence between ϵ and β_c can be derived by examining the discriminant of the cubic relation given by equation (89), which determines the transformation of complex conjugate solutions (oscillatory mode) to two real valued solutions. This discriminant (Abramowitz & Stegun 1965), to leading order in ϵ, is found to be

$$k \approx \frac{s_1^3}{27} - \frac{s_1^2 s_2^2}{108} - \frac{s_o s_1 s_2}{6} + \frac{s_o^2}{4} , \tag{96}$$

which shows that the deviation of k from its value in the adiabatic limit is of order ϵ^2 and higher; thus, the nonadiabatic contributions to the frequencies of the oscillatory mode are of at least order 2 in ϵ, as also noted earlier from the solutions (94), which are of order ϵ. The points in the $\epsilon - \beta$ space at which the oscillation frequency becomes zero and the convective mode sets in are given by $k = 0$. Thus, the loci of solutions $k = 0$ in the $\epsilon - \beta$ space demarcate the stable tubes from the convectively unstable ones. Examination of the various terms in equation (96) for k shows that the second term takes very small values compared with the other ones in the relevant range of values for β and thus can be neglected. The relation between ϵ and the critical values of β that satisfies $k = 0$ can then be written as

$$\epsilon^2 = -\frac{s_1^3 \delta_c^2}{9b_o[48b_o - 8(1 + \beta/2)s_1]} . \tag{97}$$

With ϵ expressed in terms of the radius a of the flux tube, using the definitions given by equations (49) and (50), the above equation gives a relation between tube radius a and the critical β needed for convective stability. Using flux conservation (eq. [5]) and the assumed constancy of β over depth z, the photospheric radius a_o can be related to a (thus ϵ) that corresponds to the particular location at which the instability is driven, as follows (Venkatakrishnan 1986):

$$a_o = \left(\frac{p}{p_o}\right)^{1/4} , \quad a = \left(\frac{p}{p_o}\right)^{1/4} \left(\frac{\tau_d \kappa_r}{\epsilon}\right)^{1/2} , \tag{98}$$

where $\kappa_r = K/\rho c_v$ is the thermometric conductivity. The above equation, with ϵ as given by equation (97) substituted into it, gives the relation that demarcates stable tubes from the unstable ones in terms of photospheric radius a_o and the field strength (with β converted to field strength).

Application of the relations given by equations (97) and (98) to solar flux tubes requires appropriate values for the various parameters that characterize the solar superadiabatic surface layers. Furthermore, these parameters (K, δ, H, etc.) vary steeply in the driving regions. We fix δ by requiring that the adiabatic stability condition $S_1 = 0$ yield a critical value of $\beta \approx 1.5$ that is consistent with the result that we obtain, later in § 4.1 (see also Spruit & Zweibel 1979), numerically for a realistic solar model described in § 2.2; we also show, in § 4.1, that the displacement eigenfunction for the convective downflow peaks at a depth of about 100 km from the surface. Choosing $H = 200$ km, which corresponds to layers at a depth around $z = 100$ km, and with a depth extension of $D = 1200$ km for the flux tube, we find that $\delta \approx 0.25$ in $S_1 = 0$ yields the desired value of β for adiabatic stability. The representative value for the thermometric conductivity is found to be $\kappa_r \approx 10^{10}$ cm^2 s^{-1}. Using the above chosen values for the various quantities, the relationship between photospheric tube radius a_o and field strength B_o, which demarcates the convectively stable flux tubes from those unstable, as determined by equations (97) and (98), is shown in Figure 4. The region above the curve is unstable, and that below it is stable. It is seen that tubes of radii above about 100 km have field strengths above 1 kG, with the field strength weakly dependent on a, whereas smaller tubes have a large range in the field strength from about the equipartition value of 400 G to 1 kG. These smaller tubes thus represent the regime in which radiative heating from the surroundings is capable of inhibiting their collapse. Larger tubes experience ineffective

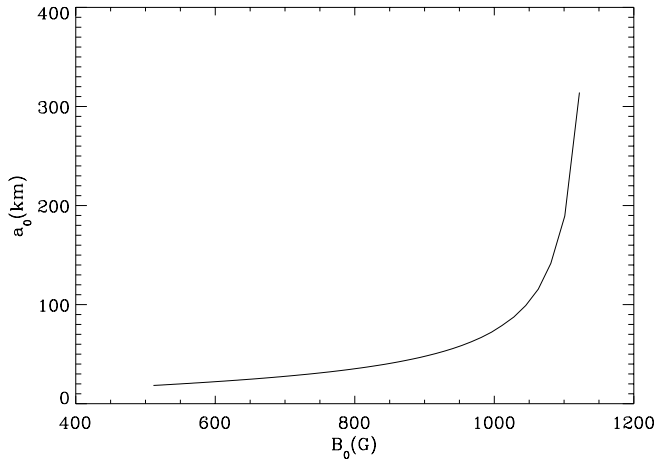

FIG. 4.—Photospheric radius a_o (km) of the flux tubes as a function of their field strengths B_o (G), as determined by equations (97) and (98) using values for the various quantities representative of the solar surface layers. This relation demarcates the convectively stable flux tubes from the unstable ones; the region above the curve is unstable, while that below the curve is stable.

heating within the dynamical collapse timescale and thus undergo collapse almost adiabatically achieving a field strength close to that set by the adiabatic limit.

3.2.1. *Effects of Vertical Radiative Losses*

In the solar surface layers the most vigorous convective motions coincide with the very rapid radiative cooling in these layers (Rimmele et al. 1995; Rast & Toomre 1993; Stein & Nordlund 1998). Figures 1 and 2 show that the superadiabaticity δ and the radiative losses (measured by $\nabla \cdot \boldsymbol{F_R}$) peak in the same region. The convective collapse of the flux-tube–confined gas in these layers is also expected to be similarly affected by the radiative losses as are the granular convective motions. Such effects are brought out in a simple way in the dispersion relation (76), where the quantities σ_2 and σ_o contain the contributions from the vertical radiative losses through the radiative loss function Q_r. Examining the various terms in the expressions for σ_2 and σ_o, we find that the dominant contributions are from Q_r leading to the simplifications

$$\sigma_2 \approx -2Q_r - \frac{1+\beta}{2}\,, \tag{99}$$

$$\sigma_o \approx Q_r\,. \tag{100}$$

As Q_r is negative, with roughly a value of -5 that corresponds to the solar superadiabatic surface layers, σ_2 is always positive for the relevant range of values of β and σ_o is always negative. The magnitude of the vertical radiative effects is controlled by C, the ratio of the local dynamical to the thermal timescale, which multiplies the above described quantities in the relation (76). This quartic relation is best solved numerically, but before doing that, we analyze its approximate solutions obtained to first order in C and ϵ. By expanding the solutions of the quartic equation (76) about the solutions of the cubic equation obtained by putting $C = 0$ in it, it is easy to check that the solutions of (76) to first order in C and ϵ are

$$\Theta_{1,2} = (\Theta_i)_{1,2} + \theta_c = \Theta_{\rm ad} + \frac{S_0 - S_1 S_2}{2S_1} + \frac{S_1 S_4}{2}\,, \tag{101}$$

$$\Theta_3 = (\Theta_i)_3 - \frac{\sigma_o}{S_1}\,C = -\frac{S_0}{S_1}\,, \tag{102}$$

where

$$\theta_c = \left(S_1\,\sigma_4 - \sigma_2 + \frac{\sigma_o}{S_1}\right)\frac{C}{2} \tag{103}$$

is the correction to order C introduced solely by the vertical radiative transfer to the adiabatic eigenvalues $\Theta_{\rm ad}$. The fourth solution of the quartic relation, which represents a thermal mode arising purely out of inclusion of the vertical radiative transfer, is given by (to order ϵ and C)

$$\Theta_4 = -\frac{1}{S_4} + \epsilon\eta_2\,. \tag{104}$$

The solutions given by equation (101), in combination with the relations given by equations (99) and (100), which establish the signs of σ_o and σ_2, show that, since S_4 is negative, oscillations in a convectively stable (positive S_1) tube are damped (θ_c is negative) by vertical radiative losses; the convective instability (negative S_1) is enhanced (θ_c is positive), if the following condition is satisfied:

$$S_1\,\sigma_4 + \frac{\sigma_o}{S_1} > \sigma_2\,. \tag{105}$$

Since the magnitude of S_1 is of the order of the superadiabaticity δ, which is always less than 1, and the magnitudes of σ_2 and σ_o are of the same order, the above condition is always satisfied in the presence of convective instability, which consequently is always enhanced by vertical radiative losses. Thus, the growth rates of the convective instability are higher by the amount θ_c than the adiabatic values, and hence the associated downflows develop faster than the adiabatic downflows, in the presence of vertical radiative losses. It is also clear that the lateral heating and the associated inhibition of convective downflow are countered by the radiative losses.

Considering the thermal mode given by (102), it is seen that, in the absence of vertical radiative losses (i.e., when $S_0 = s_o$), as discussed earlier (see the discussion next to eq. [95]), the mode is damped for convectively stable tubes (positive S_1); however, vertical losses can destabilize this mode when S_0 becomes negative (i.e., when $|C\sigma_o| > |\epsilon\eta_o|$) for a convectively stable tube (positive S_1). Thus, the nature of this thermal mode depends on the stratification and on whether the radiative losses or heating (horizontal) dominate: for convectively stable stratification (strong tubes) vertical losses destabilize the mode while horizontal heating stabilizes it, and for convectively unstable stratification (weak tubes) the horizontal heating destabilizes the mode while the vertical losses stabilize it; the instability takes the form of a slow downflow in the former case and of a slow upflow in the latter.

We now present numerical solutions of equation (76), using the following choice of parameters to represent the superadiabatic layer (driving the instability) on the Sun: $\delta \approx 0.25$, $H = 200$ km, and $Q_r = -5$. The values for the dynamical timescale τ_d and the thermal timescale $\tau_{\rm th}$ are found to be about 27 and 7000 s, respectively, at about a depth of $z = 100$ km, leading to a value of $C = 0.004$. For this set of parameters, the scaled growth rates Re(Θ) as a function of ϵ for different values of the magnetic field strength (parameterized by β) are shown in Figure 5, for

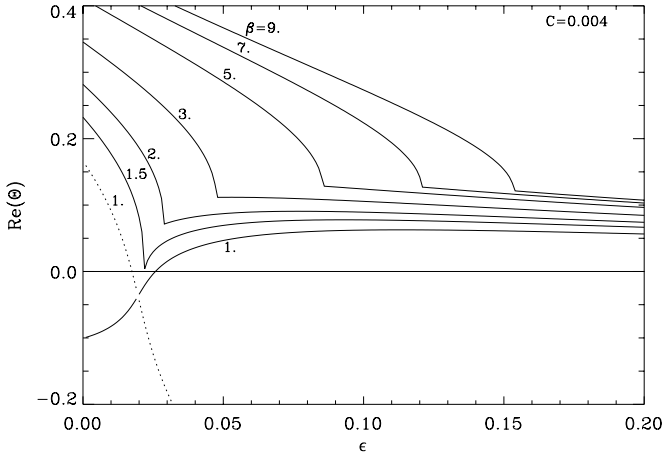

FIG. 5.—Re(Θ), i.e., growth rate scaled by the inverse of free-fall time τ_d, as a function of ϵ for different values of β; the numbers by the side of the curves denote β values. The dotted curve represents a thermal mode that becomes unstable in thick (small ϵ) and strong (small β) convectively stable flux tubes.

$D = 1200$ km. The cusps in the curves mark locations where the overstable mode is transformed into the convective mode. In terms of the solutions given by equation (101) to first order in ϵ and C, these are the points where the coefficient S_1 changes sign. However, as we showed earlier, the locations of these cusps in the ϵ–growth rate space as a function of β is a higher order effect (at least of order 2 in ϵ and C). It should be noted that the destabilization in the form of a monotonic growing mode that appears in the regime of strong fields (small β) and thick tubes (small ϵ), shown in Figure 5 as a dotted part of the curve for $\beta = 1$, is due to a thermal instability caused entirely by vertical radiative losses. This is the mode given by the solution (102), which becomes unstable for positive S_1 (convectively stable stratification or strong tubes) and negative S_o (vertical losses dominant). This purely thermal instability is related to a similar instability first studied by Defouw (1970). Now, to obtain a size-strength relation that demarcates the convectively stable flux tubes from the unstable ones from the

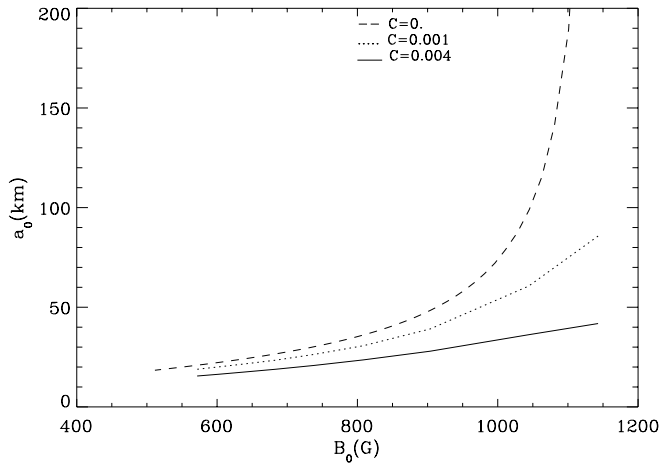

FIG. 6.—Comparison of size-strength relations obtained without vertical radiative losses ($C = 0.$; *dashed curve*) with those with the losses: the dotted curve is for $C = 0.001$ and the solid curve is for $C = 0.004$. The larger the value of C, the stronger are the effects of vertical radiative transport and cooling.

results shown in Figure 5, we note the values of ϵ and β that correspond to the cusps that mark the locations of the transition from the overstable mode to the convective mode. We then use equation (98) to obtain the relation between the photospheric size (a_o) and field strength (B_o). These relations are shown in Figure 6; for comparison we have also shown the relation obtained analytically (*dashed curve*) in § 3.2 for the case $C = 0$ (no vertical radiative transport) and that obtained for the case of $C = 0.001$ (*dotted curve*). Figure 6 clearly shows the physical implications of the vertical radiative losses for the formation of strong tubes by convective collapse; in the presence of vertical radiative losses strong fields are obtained for tube sizes that are much smaller than those that are needed in the absence of them.

4. NUMERICAL SOLUTIONS

Having identified in the previous section the physical effects of vertical radiative transport on the convective and oscillatory instabilities using a simple quasi-adiabatic analysis, we now turn to the numerical solutions of the full nonadiabatic sets of equations (38)–(41) and (60)–(63) applicable in the diffusion and Eddington approximations, respectively. These linear sets of equations are solved numerically by approximating the derivatives by finite differences. The insertion of the boundary conditions, which are stated below, in the difference equations leads to a homogeneous, tridiagonal system of equations, which constitute a generalized eigenvalue problem for the complex eigenvalues. The eigenvalues are determined by finding the roots of a determinantal equation. Muller's method is used for locating the complex roots. Determinants are evaluated efficiently using Gaussian elimination with partial pivoting, and the eigenvectors are calculated using inverse iteration (Wilkinson & Reinsch 1971).

4.1. *Boundary Conditions*

4.1.1. *Choice of Lower Boundary Mechanical Condition*

Before presenting the fully nonadiabatic solutions, we clarify the effects of open and closed mechanical conditions at the lower boundary on the convective and oscillatory motions in the flux tube. To this end, it is sufficient to consider the adiabatic and Newton's law of cooling limits. By open or closed mechanical condition we mean $d\xi/dz = 0$ or $\xi = 0$, respectively. We adopt a closed mechanical condition at the top boundary, i.e., at $z = z_{\rm top} = -500$ km, as we find that the differences in the instability growth rates or frequencies between the two cases of open or closed condition at $z_{\rm top}$ are very small; this pertains to the fact that the mass content of the gas in this location is very small. However, the location and nature of the mechanical condition at the lower boundary have dynamical consequences for both the convective and oscillatory motions. The adiabatic behavior is summarized in Figures 7 and 8, which show the eigenvalues ($\omega = \sigma_f + i\eta$) and eigenfunctions ($\xi$), respectively; η is the growth rate, and σ_f is the frequency of the mode; curves annotated as '*ob*' and '*cb*', respectively, correspond to open and closed boundaries at $z = z_b$. For a closed boundary at $z_b = 5000$ km, we find a critical value of $\beta_c = 1.64$ for convective stability (tubes with $\beta < \beta_c$ are stable) corresponding to a photospheric field strength of 1430 G, for the solar model used here. We note that Spruit & Zweibel (1979) found $\beta_c = 1.83$ (1350 G). The values of β_c obtained for the two different locations of z_b, namely, 5000

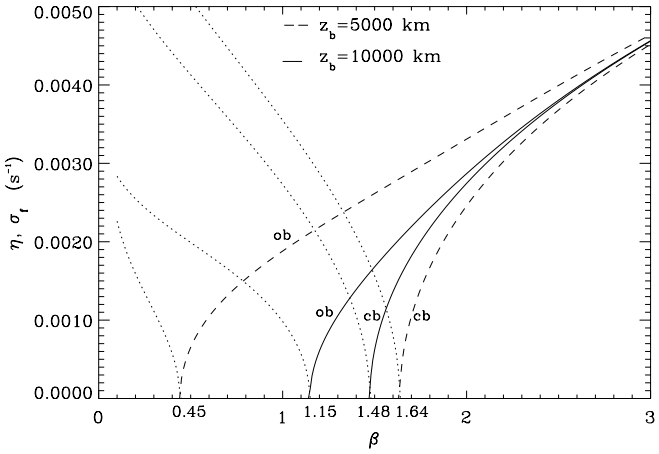

FIG. 7.—Comparison of the growth rates and frequencies (*dotted curves*) for the adiabatic case for different boundary conditions; "ob" and "cb" refer to open and closed boundaries, respectively.

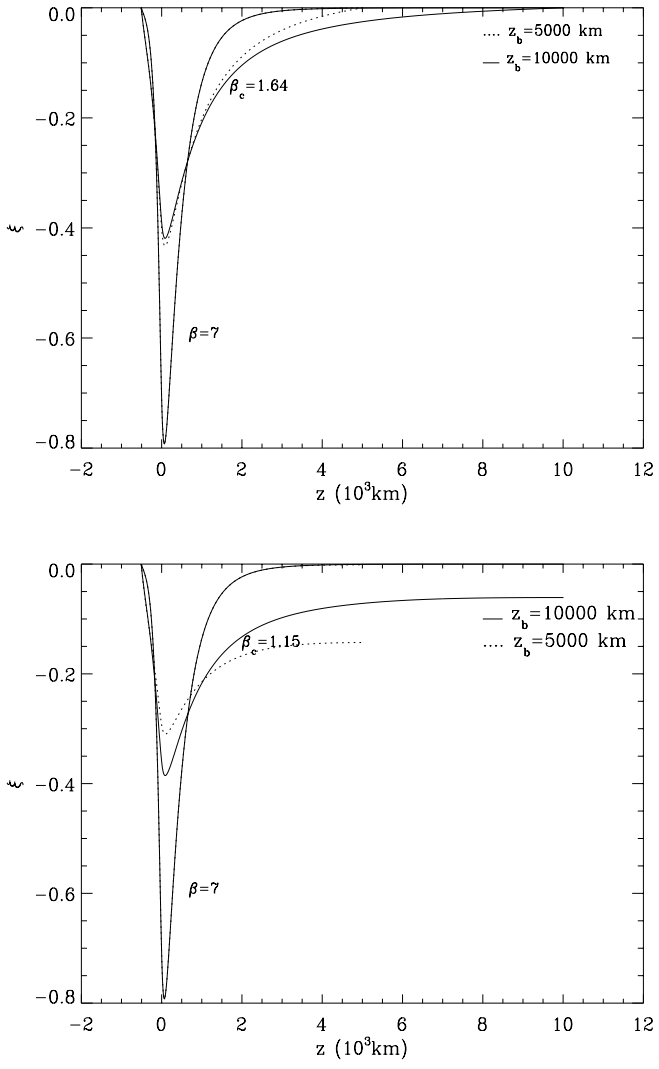

FIG. 8.—Comparison of the displacement eigenfunctions ξ for the two different depths of the lower boundary, which is (*top*) closed and (*bottom*) open. The dotted curves are for a depth of 5000 km, while the solid ones are for 10,000 km. For $\beta = 7$, i.e., for a weak-field (equipartition) tube, the two cases are indistinguishable in both open and closed boundary cases.

and 10,000 km, with open and closed conditions (as marked in Fig. 7) demonstrate that the deeper layers make a small contribution to the convective instability, which is driven mainly by the superadiabatic region confined to about 1000 km below the surface. This is also evident from the shape of the displacement eigenfunctions ξ shown in Figure 8. In general, we find that *the shallower the tube, i.e., the closer the bottom boundary to the driving regions, the larger the difference between the cases of open and closed conditions.* Figure 8 also shows that weaker tubes (e.g., $\beta = 7$) are far less sensitive to the nature of the lower boundary. Since, before collapsing to form stronger tubes, all tubes are expected to be at an initial strength of roughly about the equipartition value (around $\beta = 7$), one can conclude that the effect of the lower boundary condition is small, provided it is located sufficiently far away from the regions driving the instability.

The way the oscillatory overstable motions are affected by the conditions at the lower boundary is shown in Figure 9, which contains the eigenvalues of oscillatory and convective modes obtained when there is horizontal heat exchange based on Newton's law of cooling. The results shown are for a tube of photospheric ($\tau_e = 1$) radius $a_o = 100$ km. Similar to the adiabatic case, there is a destabilizing action of the open boundary on the convective motions, as seen from the shift of the bifurcation marking the onset of convective instability toward smaller values of β. Importantly, it is found that the overstability persists even for the open boundary, though there is a small reduction in the growth rates compared with the closed boundary case. This substantiates the result (Hasan 1986) that overstability is the physical consequence of the lateral exchange of radiation by the tube with the surroundings rather than being due to reflection associated with a closed mechanical condition at the bottom boundary, as claimed by Takeuchi (1995). We refer the reader to the original physical explanations (Cowling 1957; Moore & Spiegel 1966), which hold here as well, for the mechanism by which overstability is brought in Rajaguru (1999).

4.1.2. *Boundary Conditions for the Sets of Equations* (38)–(41) and (60)–(63)

Based on the arguments presented in the preceding subsection, we find that it is adequate to integrate the fourth-

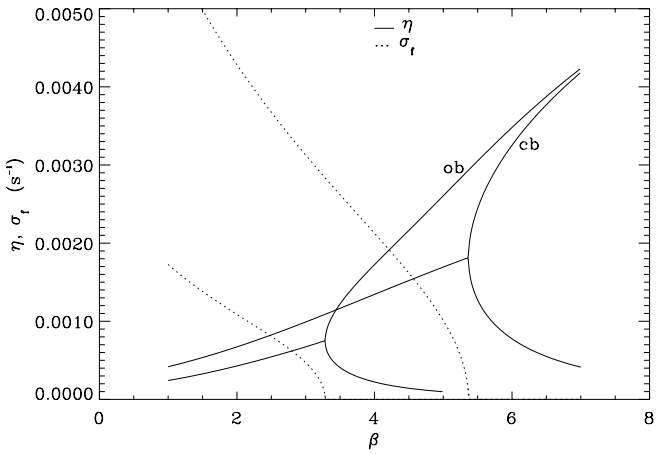

FIG. 9.—Comparison of the growth rates (*solid curves*) and frequencies (*dotted curves*) of the modes for closed bottom (cb) and open bottom (ob) boundaries; the radiative exchange is solely in the horizontal direction based on Newton's law of cooling.

order system of nonadiabatic equations only up to a depth of 5000 km with closed mechanical conditions at both the boundaries. These conditions are expressed as

$$\xi = 0\,, \quad \text{at} \quad z = z_{\rm top} \quad \text{and at} \quad z = z_b\,, \tag{106}$$

where $z_{\rm top} = -500$ km and $z_b = 5000$ km. The other two conditions required are thermal. For the diffusion approximation case, the vertical flux perturbations at $z = z_{\rm top}$ obey

$$\frac{F_z'}{F_z} = 4\,\frac{T'}{T}\,, \tag{107}$$

and at $z = z_b$ the perturbations are assumed to obey the adiabatic condition,

$$\frac{T'}{T} = \frac{\gamma - 1}{\gamma}\,\frac{p'}{p}\,. \tag{108}$$

In the Eddington approximation case, we require that there be no incoming radiation from above at $z_{\rm top}$:

$$\mathscr{H} = \frac{J}{\sqrt{3}}\,, \tag{109}$$

which on linearization gives

$$\frac{\mathscr{H}'}{\mathscr{H}} - \frac{J'}{J} = 0\,, \tag{110}$$

and at z_b, since the matter is optically thick, we assume that the mean intensity perturbations exactly equal the perturbations in the Planck function (i.e., source function),

$$\frac{S'}{S} - \frac{J'}{J} = \frac{\mathscr{H}'}{\mathscr{H}} = 0\,. \tag{111}$$

4.2. *Results and Discussions*

We now present numerical solutions of equations (38)–(41) and (60)–(63). Figure 10 and the upper panel of Figure 11 depict the growth rates (η) of the fundamental mode as a function of photospheric radius a_o of the tube; in Figure 10, the dotted curves are for the case of solely horizontal exchange under Newton's law of cooling and the solid curves are obtained in the case of diffusion approximation with radiative losses (eqs. [38]–[4]); the upper panel of Figure 11 contains a comparison of the growth rates obtained in the Eddington (*solid curves*) and diffusion (*dashed curves*) approximations and the lower panel of Figure 11 the corresponding frequencies, (σ_f), of the modes. Various curves in the figures correspond to different values of β that label each curve. The cusps in the growth rate curves shown in these figures mark the locations where the overstable mode gets transformed into the convective mode; at these points of transformation there also appears a thermal-convective mode, whose presence and behavior was discussed in § 3.2. This mode branches out, and its growth rates decrease as a_o increases; this thermal-convective mode is not shown in the figures for clarity and since our focus is on the convective and overstable modes.

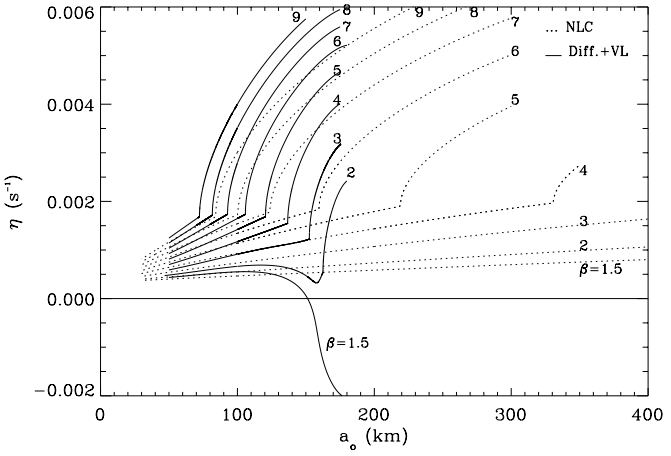

FIG. 10.—Growth rates of the convective and overstable modes as a function of surface radius a_o for various values of β; the dotted curves are for the case of radiative exchange solely in the horizontal direction, based on Newton's law of cooling, while the solid curves are obtained when full nonadiabaticity due to vertical losses is also taken into account using the diffusion approximation.

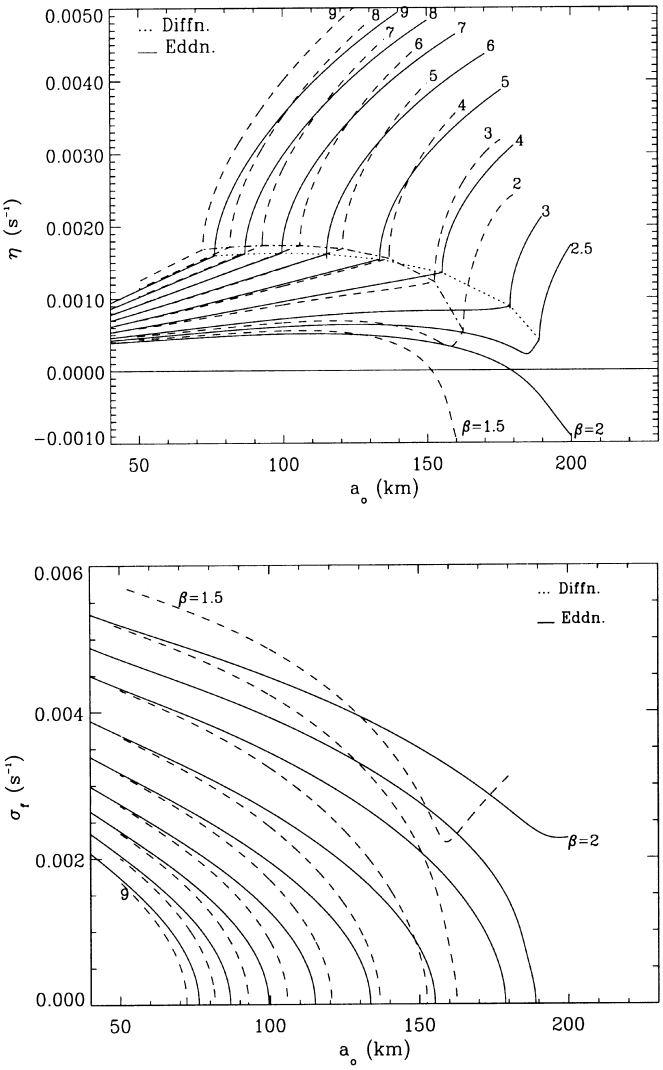

FIG. 11.—*Top*, growth rates of convective and overstable modes (fundamental mode) as a function of surface (photosphere) radius a_0 (at $\tau_e = 1$) of flux tube and *bottom*, the corresponding frequencies, for various values of β. The numbers by the side of the curves denote β values. The solid curves are obtained in the Eddington approximation, and the dashed ones correspond to the diffusion approximation.

4.2.1. *Convective Instability*

Let us first focus on the pattern of the convective instability of the tube as a function of the tube radius and field

strength (parameterized by β). The heating by radiation from the surroundings reduces the degree of adiabaticity of the downflowing gas resulting in its deceleration, and this effect, as one would naturally expect, depends on the horizontal optical thickness of the tube. There are two aspects to the stabilizing action of radiation against buoyancy forces that drive the convective instability: first, for a given initial field strength (i.e., for a curve in Fig. 10 or the upper panel of Fig. 11 for a fixed β) the lateral radiative heating that counteracts the convective force is greater for tubes with smaller radii and hence the growth rate of the convective instability decreases as the radius decreases until a critical value for the tube radius where the convective mode is transformed into an oscillatory overstable mode. Second, for a given tube radius, the lateral radiative exchange time is smaller for stronger tubes leading to an increased stabilizing action of the radiation. This requires that the critical radii for the onset of the convective instability increase as the field strength increases. The above two features are clear in Figure 10 and the upper panel of Figure 11.

The above aspects are related to the horizontal radiative exchange that counteracts the convective instability. The differences brought out in the present study, as shown in Figure 10, are mainly due to the vertical exchange and the radiative losses. As is evident in the figure, the vertical losses tend to enhance the convective instability: cooling of the gas associated with the vertical radiative losses accelerates the downflow perturbation, and hence a tube is more unstable than in the situation where the only radiative interaction is the heating due to the lateral influx of radiation. Indeed, it is the cooling associated with the radiative losses that triggers the downflow, as first discussed by Parker (1978). As such, in the absence of vertical radiative losses, convective perturbations are bidirectional: an upflow perturbation is equally unstable as a downflow, and thus an initial tube configuration is equally liable for a dispersal as it is for a collapse. However, in the presence of a net radiative loss in the vertical direction, a fluid element is always cooled irrespective of whether it moves downward or upward. This means that the motion in a direction opposite to the direction of radiative losses, i.e., the downward motion, is more unstable than the upward. As a result, downflow perturbations are amplified faster. From Figure 10, it is seen that the convective instability is not only more vigorous in the presence of vertical radiative transport (*solid curves*) but also sets in at smaller critical radii a_o than that happens when only horizontal exchange is included (*dotted curves*). Thus, it can be concluded that in the presence of vertical radiative losses a weak-field tube preferably undergoes a collapse resulting in its field intensification rather than an upward convective perturbation that tends to further weaken and disperse the tube.

Now, comparing the diffusion and Eddington approximations shown in Figure 11, it is seen that the growth rates obtained in the latter case are appreciably smaller than those in the former. Moreover, for a given value of β, i.e., for a tube of given field strength, the onset of convective instability requires a larger size tube in the Eddington approximation than that required in the diffusion approximation. We attribute these effects to the overestimate, in the diffusion approximation, of radiative losses in the upper photospheric and higher layers that are optically thin. It is also found that the differences between the two approximations are larger for smaller values of β, i.e., for stronger tubes. This is easily explained because stronger tubes are more transparent to radiation than the weaker ones, and hence the diffusion approximation underestimates the horizontal heating effects. As noted earlier, one of the quantities that measures the deviation from the diffusion approximation is Δ_c, the ratio of the difference between the mean intensity and the Planck function to the Planck function. The variation of this quantity over depth for different values of β is shown in Figure 3. This quantity has finite values only in the layers around $\tau_e = 1$ and above and also is larger for smaller values of β, i.e., for stronger tubes; since the vertical losses, which destabilize the convective mode, are overestimated by the diffusion approximation in the same layers, it is clear that Δ_c stabilizes the convective mode. The physical manifestation of such differences between the diffusion and Eddington approximations is that the convective instability is more vigorous in the former case. The convective instability is completely suppressed for tubes with $\beta < 2.45$ irrespective of size, in the Eddington approximation. This corresponds to a field strength of about 1160 G at $\tau = 1$ inside the tube. This has to be compared with the value of 1310 G ($\beta = 1.9$) that is obtained in the diffusion approximation and the value of 1430 G ($\beta = 1.6$) for the adiabatic case. The above numbers clearly demonstrate the stabilizing aspects of the radiation on the convective instability of the tube. We point out here that the field strength of 1160 G that we obtain here does not necessarily imply that all collapsing tubes of weaker fields will attain this unique value and become stable. This value represents a necessary strength for stability against convective collapse and thus can be considered as a minimum strength for stability. A collapsing weaker tube of sufficient size can of course attain an equilibrium collapsed state of field strength higher than this value (Spruit 1979).

4.2.2. *Size (Flux)–Field Strength Relation*

The relation between critical photospheric radii a_o and field strengths $B_{\rm ph}$, which demarcate the convectively stable flux tubes from the unstable ones, is obtained by selecting the values of β and a_o that correspond to the convective onset points in the growth rate curves of Figure 10 and the upper panel of Figure 11. The resulting radius–field strength relations, corresponding to different approximations, are shown in the upper panel of Figure 12. The best observations available so far on the small-scale magnetic fields do not achieve high enough resolution to resolve the individual magnetic features and thus cannot determine their intrinsic sizes directly. They measure only the magnetic fluxes and the strengths and their distribution (Lin 1995; Solanki et al. 1996). Hence, for comparison, we have shown the corresponding magnetic flux–field strength relations in the lower panel of Figure 12. The dashed, dotted, and solid curves, in Figure 12, correspond to Newton's law of cooling, diffusion, and Eddington approximations, respectively. Flux tubes of strengths and fluxes (sizes) that fall to the right of the flux (size)-strength relation curves of Figure 12 are stable. In deriving such relations between the size and the field strength and comparing them with the observed distribution on the Sun's surface, the following scenario is implicitly assumed: an initial weak-field tube of size (radius) large enough to be convectively unstable, i.e., a tube on a location beyond the convective onset points toward larger radii on the curves of Figure 10 and the upper panel of Figure 11, would collapse leading to an increase in its strength (lower

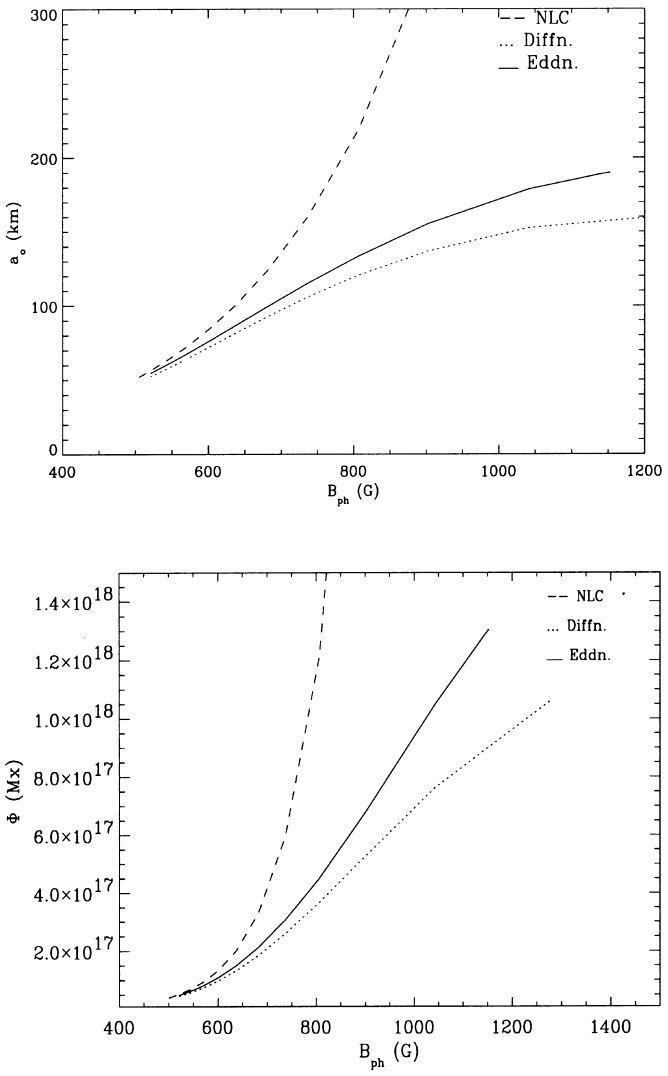

FIG. 12.—*Top*, size-strength and *bottom*, magnetic flux–strength relations, which demarcate the convectively stable flux tubes from the unstable ones at the solar photosphere. The region to the right of these curves is stable and that to the left is unstable. Different curves correspond to different approximations for the radiative effects, as marked in the figure.

β) and a decrease in its size, on account of magnetic flux conservation; if, in this process, a collapsing tube attains a size and strength such that it crosses the convective onset points of the curves of Figure 10 and the upper panel of Figure 11 and reaches the convectively stable regions, then the collapse is assumed to cease and attain its final equilibrium state, thereby leading to the predicted distribution shown in Figure 12. Hereafter, in deriving further results and conclusions, we refer to values obtained in the Eddington approximation, as it is the most realistic of all the cases we have treated. It is found that the maximum possible initial field strength (B_c) up to which a tube is subject to the convective instability is about 1160 G, corresponding to $\beta = 2.45$ and a critical size $a_c = 190$ km; i.e., a tube of strength 1160 G can still collapse to a higher strength if its size is greater than $a_o = 190$ km. Thus, using these values, we conclude that *there is a critical value of magnetic flux* $\Phi_c = \pi B_c a_c^2 = 1.31 \times 10^{18}$ Mx *above which all flux concentrations attain always a collapsed state of strong kilogauss field above* 1160 G. This result is in excellent agreement with the observational results (Solanki et al. 1996; Lin 1995; Keller et al. 1994). Realistically, in the absence of any other mechanism to form stronger tubes, the maximum attainable field strength (corresponding to the maximum observed granular speed of about 3 km s^{-1}) is the equipartition strength around 500 G, corresponding to a value of $\beta = 9$. Thus, all initial equipartition strength magnetic flux concentrations with fluxes less than the above obtained limit of 1.31×10^{18} Mx are subject to the radiative inhibition effects as brought out in the present study, and consequently they would exhibit the *flux-strength* relation that is obtained here.

4.2.3. *Overstability*

Overstable oscillations are characterized by the appearance of complex conjugate pairs of eigenvalues for Ω. In Figure 10 and the upper panel of Figure 11, the overstable modes correspond to the portions to the left of the cusps in the curves. As is well known (Cowling 1957; Moore & Spiegel 1966), the overstability of wave motions is due to a delicate phasing of horizontal radiative exchange with the restoring and driving forces of the oscillating fluid elements. In essence, energy is extracted from the radiation and converted into mechanical oscillations. For a flux tube, the horizontal radiative exchange with the surroundings makes the oscillations grow (Hasan 1986). Here we concentrate on the effects imparted by vertical radiative transport. It is seen that the growth rates of the overstable mode of a flux tube, which can undergocollapse for radii a_o larger than a critical value, are larger when there is vertical radiative transport than when it is not present. In other words, weaker but convectively stable smaller size tubes, whose interior is not thermally much different from the surroundings, extract more energy from the radiation when there is vertical transport than when it is not present. We attribute this effect to the opacity perturbations (κ mechanism) associated with the thermal perturbations, which are brought in automatically through the inclusion of vertical flux perturbations. Now, considering the differences between the diffusion and Eddington approximations, it is found that (Fig. 11, *upper panel*) the latter reduces the growth rates of the overstable oscillations. We interpret this again as an effect of Δ_c, i.e., the mean intensity J being different from the Planck function S. Such a stabilizing influence of Δ_c has been found also in studies of radiative transfer effects on the stability of the solar p-modes (Christensen-Dalsgaard & Frandsen 1983).

The behavior of the overstable mode in strong and convectively stable flux tubes is shown in Figure 13, choosing values of β representative of solar network elements. Shown are the growth rates as a function of a_o, in the diffusion (*dotted curves*) and Eddington (*solid curves*) approximations. For a_o greater than about 120 km, it is seen that the growth rates go down sharply and become negative above certain critical values of a_o that depend on β. This damped behavior of the mode is purely due to the effect of vertical radiative losses, as it is not present in their absence. We explain this feature as due to an asymmetry between the downward and upward swings of an oscillating fluid element, introduced by net radiative losses in the vertical direction: the upward return passage of an initial downward motion of the fluid element is now not as fast as would occur in the absence of vertical losses. In other words, there is a reduction in the energy gained by the fluid element from the radiation field (from horizontal exchange), and hence the oscillations experience less amplification. This is

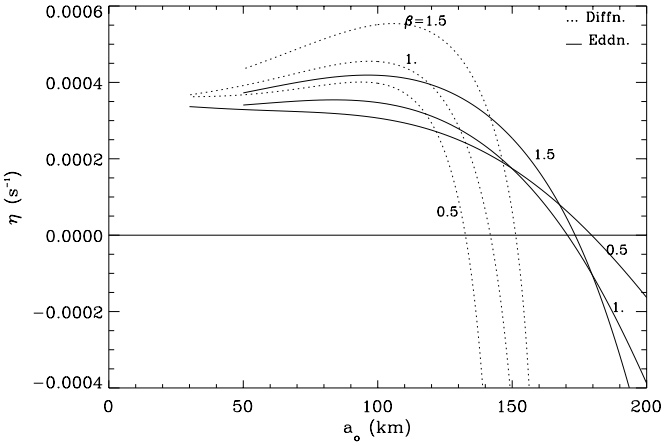

FIG. 13.—Comparison of growth rates of the overstable mode in the diffusion (*dotted curves*) and Eddington (*solid curves*) approximations, for convectively stable tubes. The numbers by the side of the curves denote β values.

nothing but the well-known phenomenon of radiative damping. From the results shown in Figure 13, we see that such radiative damping effects associated with vertical losses are greater for a tube with a strong magnetic field. Since a stronger tube is more evacuated than a weaker one, the vertical loss timescale in it is now much shorter, resulting in greater damping of the oscillations. This effect is further enhanced as the tube size increases, which reduces the horizontal heating effects. Thus, tubes that are strong enough with sizes larger than a critical value of a_o about 170 km (for $\beta \approx 0.5$) are subject to the severe radiative damping associated with the vertical radiative losses and thus are stable. We identify the solar network elements with such tubes.

5. CONCLUSIONS

We have modeled the interaction between the radiation and gas motions in magnetic flux tubes extending vertically through the solar surface layers. Very rapid radiative cooling in the photospheric and subphotospheric regions has been observed (Rimmele et al. 1995) to coincide with vigorous convective downflows and the associated localized events of acoustic excitations. Including radiative cooling in the quasi-adiabatic approximation, we have demonstrated in a simple manner such effects of radiative losses and their dynamical consequences on the evolution of gas confined to magnetic flux tubes. Our numerical stability analyses presented in § 4, using a realistic model of solar upper convective and photospheric layers and a refined treatment of radiative transfer, have further corroborated these results. Convective downflows are shown to accelerate faster because of the cooling associated with the vertical radiative losses thereby theoretically verifying the thermal origin of the convective collapse mechanism as the cause of intense magnetic tubes on the Sun. We have thus shown that flux tubes will preferentially undergo a collapse (downflow) because of the asymmetry between downflow and upflow perturbations introduced by vertical radiative losses. We have also shown the existence of a pure thermal instability that owes its existence entirely to vertical radiative transport; a thick tube that is not subject to efficient lateral radiative heating, but in which vertical radiative losses occur, is shown to develop a downflow because of this instability. We point out that the presence of a collapsed strong flux tube in an intergranular region is most likely to enhance further the radiative cooling in its immediate environment thereby producing much cooler and vigorous downflows that give rise to the acoustic events observed by (Rimmele et al. 1995).

We have obtained a critical limit for the magnetic flux on the solar surface that demarcates the small-scale flux concentrations into two groups: (1) flux concentrations with fluxes above this limit of about 1×10^{18} Mx collapse unhindered attaining field strengths greater than 1160 G; (2) flux concentrations with fluxes smaller than the above limit are subject to the inhibiting action of the radiation field. We identify the strong-field solar network magnetic elements with flux tubes in the first group; the network elements have the property that their field strengths, which are between 1200 and 1500 G, are weakly dependent on their magnetic flux content (see the review by Schüssler 1992; Solanki et al. 1996), which is greater than about 10^{18} Mx. Our results show that these network tubes are all fully collapsed forms of initial, sufficiently thick flux tubes that undergo a radiatively unhindered collapse process. The flux tubes in the second category above are identified with the weak and moderate field strength intranetwork structures; these structures are subject to radiative inhibiting action of varying degree on the collapse process, depending on their size, and as a result exhibit the *flux* (*size*)-*strength* relations derived in this paper (§ 4.2.2); such relations compare well with the observations (Solanki et al. 1996; Lin 1995). The above explained broad agreement between our theoretical predictions and observations suggests that the convective collapse is indeed the process responsible for forming the highly inhomogeneous small-scale structured magnetic fields on the Sun. By analogy, this same process is very likely to operate on stars like the Sun, producing similar concentrated magnetic field structures.

We have also established improved stability criteria for the overstable mode of the tube. In particular, it is shown that the wave motions of a convectively stable tube are mainly a consequence of the horizontal radiative exchange of the tube with the surroundings. A closed mechanical boundary condition at the bottom is *not the cause of overstability*, though overstable growth rates are slightly reduced for an open boundary. The influence of the open bottom boundary is negligible on the convective instability of the tube provided the location of the bottom boundary is deep enough and far away from the driving regions, which are mainly confined to regions of depth about 1000 km from the surface ($\tau_e = 1$). Furthermore, we have demonstrated that strong tubes of large enough sizes are subject to radiative damping associated with the vertical radiative losses, leading to a damping of the slow magnetoacoustic mode of the tube. This leads to the conclusion that a large-sized network tube (of diameter about 300 km or higher) is not subject to the overstability due to the horizontal radiative exchange.

The first author S. P. R. is grateful to P. Venkatakrishnan for useful discussions. The computational facilities of the Supercomputer Education and Research Centre, Indian Institute of Science, Bangalore are thankfully acknowledged.

APPENDIX A

DERIVATION OF EQUATIONS IN THE QUASI-ADIABATIC APPROXIMATION

The Lagrangian perturbations in the vertical radiative flux are written, using equation (37), as

$$\frac{\delta F_R}{F_R} = \left(\frac{d\ln T}{dz}\right)^{-1} \frac{d}{dz}\left(\frac{\delta T}{T}\right) - \frac{d\xi}{dz} + \left(4 + \frac{\chi_T}{\chi_\rho} - \kappa_T\right)\frac{\delta T}{T} - \left(\kappa_p + \frac{1}{\chi_\rho}\right)\frac{\delta p}{p} . \tag{A1}$$

The estimation of $\delta F_R/F_R$ in the quasi-adiabatic approximation is done using the adiabatic relations among the variables to evaluate the right-hand side of equation (A1). This procedure yields the following approximation for the vertical flux perturbations in terms of the vertical displacement ξ and pressure perturbation $\delta p/p$:

$$\frac{\delta F_R}{F_R} = \frac{D_1(z)}{L}\,\xi + D_2(z)\,\frac{\delta p}{p} , \tag{A2}$$

where

$$D_1(z) = b_2(z) - \theta^2\tau_d^2\, b_1(z) , \tag{A3}$$

$$b_1(z) = \frac{\nabla_a}{\nabla} , \tag{A4}$$

$$b_2(z) = -\frac{(1+\beta)L}{2H}\,\frac{\delta}{\nabla} , \tag{A5}$$

and

$$D_2(z) = \frac{H}{\nabla}\frac{d\nabla_a}{dz} - \frac{\nabla_a}{\nabla} + \frac{\beta}{2}\frac{\delta}{\nabla} + \frac{1}{\Gamma_1} + \left(4 - \kappa_T + \frac{\chi_T}{\chi_\rho}\right)\nabla_a - \kappa_\rho - \frac{1}{\chi_\rho} . \tag{A6}$$

Noting that

$$\delta\left(\frac{dF_R}{dz}\right) = \frac{d\delta F_R}{dz} - \frac{dF_R}{dz}\frac{d\xi}{dz} , \tag{A7}$$

we have the energy equation,

$$\theta\,\frac{\delta s}{c_v} = -\frac{1}{\rho c_v T}\,\delta\left(\frac{dF_R}{dz}\right) - \frac{4}{\tau_R}\,\frac{\delta T}{T} + \frac{4}{\tau_R}\,\frac{d\ln T}{dz}\,\xi , \tag{A8}$$

taking the following form:

$$(\gamma\theta\tau_d + 4\epsilon)\,\frac{\delta s}{c_v} = \frac{\gamma D_3(z)}{H}\,\xi + \gamma D_4(z)\,\frac{\delta p}{p} , \tag{A9}$$

where $D_3(z)$ and $D_4(z)$ are the dimensionless functions,

$$D_3(z) = C(c(z) - \theta^2\tau_d^2\, d(z)) + 4\epsilon\nabla , \tag{A10}$$

$$D_4(z) = C(u(z) - \theta^2\tau_d^2\, w(z)) - 4\epsilon\nabla_a , \tag{A11}$$

and

$$c(z) = H\,\frac{db_2}{dz} + \frac{(1+\beta)L}{2}\left(\frac{b_2}{L} + \frac{D_2}{H}\right) + L\,\frac{d\ln F_R}{dz}\left(\frac{Hb_2}{L} - \frac{1+\beta}{2}\right), \tag{A12}$$

$$d(z) = b_1\left(\frac{1+\beta}{2} + H\,\frac{d\ln F_R}{dz}\right) + H\,\frac{db_1}{dz} + D_2 , \tag{A13}$$

$$u(z) = L\,\frac{dD_2}{dz} + \left(\frac{d\ln F_R}{dz} - \frac{2+\beta}{2H}\right)LD_2 + \left(\frac{\beta}{2} + \frac{1}{\Gamma_1}\right)\left(L\,\frac{d\ln F_R}{dz} - b_2\right), \tag{A14}$$

$$w(z) = -\left(\frac{\beta}{2} + \frac{1}{\Gamma_1}\right)b_1 . \tag{A15}$$

Substituting for the entropy perturbations in the Lagrangian form of equation (38) using equation (A9) we have, along with

the perturbed momentum equation (39), the following system of equations in the quasi-adiabatic approximation:

$$\frac{d\xi}{dz} = \left[\frac{1+\beta}{2} + \frac{\chi_T}{q\chi_\rho} D_3(z)\right]\frac{\xi}{H} - \left[\frac{\beta}{2} + \frac{1}{\Gamma_1} - \frac{\chi_T}{q\chi_\rho} D_4(z)\right]\frac{\delta p}{p}, \tag{A16}$$

$$\frac{d}{dz}\left(\frac{\delta p}{p}\right) = \left(\frac{1+\beta}{2H} - \frac{\theta^2}{g}\right)\frac{\xi}{H} - \left(1+\frac{\beta}{2}\right)\frac{1}{H}\frac{\delta p}{p}, \tag{A17}$$

where

$$q = \gamma\theta\tau_d + 4\epsilon . \tag{A18}$$

The combination of the above two equations yields the second-order equation (69) analyzed in § 3.

REFERENCES

Abramowitz, M., & Stegun, I. A. 1965, Handbook of Mathematical Functions (New York: Dover)
Antia, H. M., & Chitre, R. 1979, Sol. Phys., 63, 67
Biermann, L. 1941, Vierteljahrsschr. Astron. Ges., 76, 194
Cattaneo, F., Brummell, N. H., Toomre, J., Malagoli, A., & Hurlburt, N. E. 1991, ApJ, 370, 282
Christensen-Dalsgaard, J., & Frandsen, S. 1983, Sol. Phys., 82, 165
Cowling, T. G. 1957, Magnetohydrodynamics (New York: Wiley)
Defouw, R. J. 1970, ApJ, 160, 659
Ferriz-Mas, A., & Schüssler, M. 1989, Geophys. Astrophys. Fluid Dyn., 48, 217
Hasan, S. S. 1983, in IAU Symp. 102, Solar and Stellar Magnetic Fields: Origin and Coronal Effects, ed. J. O. Stenflo (Dordrecht: Reidel), 73
———. 1984, ApJ, 285, 851
———. 1985, A&A, 143, 39
———. 1986, MNRAS, 219, 357
———. 1988, ApJ, 332, 499
Hasan, S. S., & Kalkofen, W. 1994, ApJ, 436, 355
Hasan, S. S., Kalkofen, W., & Steiner, O. 1999, in Proc. 2d Solar Polarization Workshop, ed. K. N. Nagendra & J. O. Stenflo (Dordrecht: Kluwer), 409
Hasan, S. S., Kneer, F., & Kalkofen, W. 1998, A&A, 332, 1064
Howard, R. W., & Stenflo, J. O. 1972, Sol. Phys., 22, 402
Jones, C. A. 1970, MNRAS, 176, 145
Keller, C. U., Deubner, F.-L., Egger, U., Fleck, B., & Povel, H. P. 1994, A&A, 286, 626
Knölker, M., & Schüssler, M. 1988, A&A, 202, 275
Knölker, M., Schüssler, M., & Weisshaar, E. 1988, A&A, 194, 257
Lin, H. 1995, ApJ, 446, 421
Massaglia, S., Bodo, G., & Rossi, P. 1989, A&A, 209, 399
Mihalas, D. 1967, Methods Comput. Phys., 7, 1
Moore, D. W., & Spiegel, E. A. 1966, ApJ, 143, 871
Musman, S., & Nelson, G. D. 1976, ApJ, 207, 981
Nelson, G. D., & Musman, S. 1977, ApJ, 214, 912
———. 1978, ApJ, 222, L69
Parker, E. N. 1978, ApJ, 221, 368
Rajaguru, S. P. 1999, Ph.D. thesis, Indian Institute of Science, Bangalore
Rast, M. P., Nordlund, A., Stein, R. F., & Toomre, J. 1993, ApJ, 408, L53
Rast, M. P., & Toomre, J. 1993, ApJ, 419, 240
Rimmele, T. R., Goode, P. R., Harold, E., & Stebbins, R. T. 1995, ApJ, 444, L119
Roberts, B. 1976, ApJ, 204, 268
Roberts, B., & Webb, A. R. 1978, Sol. Phys., 56, 5
Rogers, F. J., & Iglesias, C. 1992, ApJS, 79, 507
Rybicki, G. B., & Lightman, A. P. 1979, Radiative Processes in Astrophysics (New York: Wiley)
Schüssler, M. 1990, in IAU Symp. 138, Solar Photosphere: Structure, Convection and Magnetic Fields, ed. J. O. Stenflo (Dordrecht: Reidel), 161
———. 1992, in The Sun—A Laboratory for Astrophysics, ed. J. T. Schmelz & J. C. Brown (Dordrecht: Kluwer), 191
Solanki, S. K., Zufferey, D., Lin, H., Rüedi, I., & Kuhn, J. R. 1996, A&A, 310, L33
Spiegel, E. A. 1957, ApJ, 126, 202
Spruit, H. C. 1977, Ph.D. thesis, Uttrecht Univ.
———. 1979, Sol. Phys., 61, 363
———. 1981, A&A, 98, 155
Spruit, H. C., Nordlund, A., & Title, A. M. 1990, ARA&A, 28, 263
Spruit, H. C., & Zwaan, C. 1981, Sol. Phys., 70, 207
Spruit, H. C., & Zweibel, E. G. 1979, Sol. Phys., 32, 41
Stein, R. F., & Nordlund, A. 1998, ApJ, 499, 914
Steiner, O. 1990, Ph.D. thesis, Inst. Astron., ETH Zurich
Stenflo, J. O. 1973, Sol. Phys., 32, 41
———. 1994, in Solar Magnetic Fields, ed. M. Schüssler & W. Schmidt (Cambridge: Cambridge Univ. Press), 301
Takeuchi, A. 1995, PASJ, 47, 331
Unno, W., & Ando, H. 1979, Geophys. Astrophys. Fluid Dyn., 12, 107
Unno, W., & Spiegel, E. A. 1966, PASJ, 18, 85
Venkatakrishnan, P. 1985, J. Astrophys. Astron., 6, 21
———. 1986, Nature, 322, 156
Vernazza, J. E., Avrett, E. H., & Loeser, R. 1981, ApJS, 45, 635
Webb, A. R., & Roberts, B. 1978, Sol. Phys., 59, 249
———. 1980, Sol. Phys., 68, 87
Wilkinson, J. H., & Reinsch, C. 1971, in Handbook for Automatic Computation, Vol. 2 (Berlin: Springer)